

Radical chemistry in the Pearl River Delta: observations and modeling of OH and HO₂ radicals in Shenzhen 2018

Xinping Yang^{1,2}, Keding Lu^{1,2,*}, Xuefei Ma^{1,2}, Yue Gao^{1,2}, Zhaofeng Tan³, Haichao Wang⁴, Xiaorui Chen^{1,2}, Xin Li^{1,2}, Xiaofeng Huang⁵, Lingyan He⁵, Mengxue Tang⁵, Bo Zhu⁵, Shiyi Chen^{1,2}, Huabin Dong^{1,2}, Limin Zeng^{1,2}, Yuanhang Zhang^{1,2,*}

¹State Key Joint Laboratory of Environmental Simulation and Pollution Control, College of Environmental Sciences and Engineering, Peking University, Beijing, China

²State Environmental Protection Key Laboratory of Atmospheric Ozone Pollution Control, Peking University, Beijing, China

³Institute of Energy and Climate Research, IEK-8: Troposphere, Forschungszentrum Juelich GmbH, Juelich, Germany

⁴School of Atmospheric Sciences, Sun Yat-Sen University, Zhuhai, China

⁵Laboratory of Atmospheric Observation Supersite, School of Environment and Energy, Peking University Shenzhen Graduate School, Shenzhen, China

Correspondence to: Keding Lu (k.lu@pku.edu.cn), Yuanhang Zhang (yhzhang@pku.edu.cn)

Abstract. The ambient radical concentrations were measured continuously by laser-induced fluorescence during the STORM (STudy of the Ozone foRmation Mechanism) campaign at the Shenzhen site, located in the Pearl River Delta in China, in the autumn of 2018. The diurnal maxima were $4.5 \times 10^6 \text{ cm}^{-3}$ for OH and $4.2 \times 10^8 \text{ cm}^{-3}$ for HO₂ (including an estimated interference of 23%-28% from RO₂ radicals during the daytime), respectively. The state-of-the-art chemical mechanism underestimated the observed OH concentration, similar to the other warm-season campaigns in China. The OH underestimation was attributable to the missing OH sources, which can be explained by the X mechanism. Good agreement between the observed and modeled OH concentrations was achieved when an additional numerical X equivalent to 0.1 ppb NO concentrations was added into the base model. The isomerization mechanism of RO₂ derived from isoprene contributed approximately 7% to the missing OH production rate and the oxidation of isoprene oxidation products (MACR and MVK) had no significant impact on the missing OH sources, demonstrating further exploration of unknown OH sources is necessary. A significant HO₂ heterogeneous uptake was found in this study, with an effective uptake coefficient of 0.3. The model with the HO₂ heterogeneous uptake can simultaneously reproduce the OH and HO₂ concentrations when the amount of X changed from 0.1 to 0.25 ppb. The ROx primary production rate was dominated by photolysis reactions, in which the HONO, O₃, HCHO, and carbonyls photolysis accounted for 29%, 16%, 16%, and 11% during the daytime, respectively. The ROx termination rate was dominated by the reaction of OH + NO₂ in the morning, and thereafter the radical self-combination gradually became the major sink of ROx in the afternoon. As the sum of the respective oxidation rates of the pollutants via reactions with oxidants, the atmospheric oxidation capacity was evaluated, with a peak of 11.8 ppb h⁻¹ around noontime. The ratio of $P(\text{O}_3)_{\text{net}}$ to AOC_{VOCs} , which indicates the yield of net ozone production from VOCs oxidation, trended to increase and then decrease as the NO concentration increased. The median ratios ranged within 1.0-4.5, with the maximum existing when the NO concentration was

34 approximately 1 ppb. The nonlinear relationship between the yield of net ozone production from VOCs oxidation and NO
35 concentrations demonstrated that optimizing the NO_x and VOCs control strategies is critical to controlling ozone pollution
36 effectively in the future.

37 **1 Introduction**

38 Severe ambient ozone (O₃) pollution is one of China's most significant environmental challenges (Shu et al., 2020;Li et al.,
39 2019;Wang et al., 2020;Ma et al., 2019b;Wang et al., 2017a). Despite the reduction in emissions of O₃ precursors, O₃
40 concentration is increasing, especially in urban cities. The O₃ average trends for the focus megacity clusters are 3.1 ppb a⁻¹,
41 2.3 ppb a⁻¹, 0.56 ppb a⁻¹, and 1.6 ppb a⁻¹ for North China Plain (NCP), Yangtze River Delta (YRD), Pearl River Delta (PRD),
42 and Szechwan Basin (SCB), respectively (Li et al., 2019). The nonlinearity between O₃ and precursors illustrates that it is
43 necessary to explore the cause of O₃ production. The tropospheric O₃ is only generated in the photolysis of nitrogen dioxide
44 (NO₂) which is produced as the by-product within the radical cycling. Thus, the investigation of radical chemistry is critical to
45 controlling secondary pollution.

46 Hydroxyl radicals (OH), the dominant oxidant, control the atmospheric oxidation capacity (AOC) in the troposphere. The
47 OH radicals convert primary pollutants to secondary pollutants and are simultaneously transformed into peroxy radicals (HO₂
48 and RO₂). Within the interconvert of RO_x (= OH, HO₂, and RO₂), secondary pollutants are generated, and thus the further
49 exploration of radical chemistry is significant. The radical closure experiment, an effective indicator for testing our
50 understanding of radical chemistry, has been conducted since the central role of OH radicals was recognized in the 1970s (Levy,
51 1971;Hofzumahaus et al., 2009). The underestimation of OH radicals in environments characterized by low nitrogen oxides
52 (NO) and high volatile organic compounds (VOCs) has been identified (Lu et al., 2013;Lu et al., 2012;Tan et al., 2017;Tan et
53 al., 2019;Yang et al., 2021;Hofzumahaus et al., 2009;Lelieveld et al., 2008;Whalley et al., 2011). New radical mechanisms
54 involving unclassical OH regeneration have been proposed, mainly including Leuven Isoprene Mechanism (LIM) and X
55 mechanism (Peeters and Muller, 2010;Peeters et al., 2014;Peeters et al., 2009;Hofzumahaus et al., 2009). The LIM which has
56 been integrated into the current radical mechanism is still insufficient to explain the OH missing sources. The X mechanism
57 was identified several times, but the amount of the numerical species, X, varied in different environments, and the nature of X
58 is still unknown (Hofzumahaus et al., 2009;Lu et al., 2013;Lu et al., 2012;Tan et al., 2017;Tan et al., 2019;Yang et al., 2021;Ma
59 et al., 2022a). Therefore, further exploration of radical regeneration sources is necessary.

60 Due to the strong photochemistry influenced by high temperatures and strong radiation, severe O₃ pollution appeared to
61 occur in YRD and PRD, especially in PRD (Ma et al., 2019b;Wang et al., 2017a). Radicals, the dominant oxidant in the
62 troposphere, have been measured during warm seasons in NCP (Yufa 2006, Wangdu 2014, and Beijing 2016), YRD (Taizhou
63 2018), SCB (Chengdu 2019), and PRD (Backgarden 2006, and Heshan 2014) in China (Lu et al., 2013;Lu et al., 2012;Tan et

64 al., 2017;Tan et al., 2019;Yang et al., 2021;Tan et al., 2021;Ma et al., 2022a). The radical observations in PRD, where the cities
65 are suffering from severe O₃ pollution, have not been conducted since 2014, and thus the oxidation capacity here has not been
66 clear in recent years. Therefore, we carried out a continuous comprehensive field campaign (STudy of the Ozone foRmation
67 Mechanism - STORM) involving radical observations in Shenzhen, one of the megacities in PRD, in the autumn of 2018.
68 Overall, the following will be reported in this study.

- 69 (1) The observed radical concentrations, and the comparison between the radical observations and simulations.
- 70 (2) The exploration of the unclassical OH regeneration sources based on the experimental budget.
- 71 (3) The sources and sinks of RO_x radicals.
- 72 (4) The evaluation of the atmospheric oxidation capacity.

73 2 Methodology

74 2.1 Measurement site and instrumentation

75 The STORM campaign was conducted from September to October 2018 in Peking University Shenzhen Graduate School
76 (22.60 deg N, 113.97 deg E), in the west of Shenzhen, Guangdong province. As shown in Fig. 1, this site, which belongs to
77 the urban site, is located in the university town, and is surrounded by residential and commercial areas. The northwest of the
78 site is close to the Shenzhen Wildlife Park, and the northeast is close to the Xili Golf Club (Yu et al., 2020). The Tanglang
79 Mountain Park with active biogenic emissions is located about 1 km southeast of the site. Overall, this site has no significant
80 local pollution sources nearby, but can represent the urban pollution characteristics (Huang et al., 2012a;Huang et al.,
81 2012b;Gao et al., 2018).



82
83 **Figure 1: Geographical location and surrounding environmental conditions of the measurement site in the STORM campaign (The**
84 **maps are from <https://map.baidu.com>).**

85 Most instruments were set up on the top of a four-story academic building (about 20 m). Besides HO_x radicals measured by
86 the Peking University-Laser Induced Fluorescence system (PKU-LIF) (see the details in Sect. 2.2), a comprehensive set of

87 trace gases was conducted to support the exploration of radical chemistry, including meteorological parameters (temperature,
88 pressure, relative humidity, *etc.*), photolysis frequency, OH reactivity (k_{OH}) and the trace gases (NO, NO₂, O₃, VOCs, *etc.*). k_{OH}
89 was measured by the Laser flash Photolysis-Laser Induced Fluorescence system (LP-LIF). Most of the inorganic trace gases
90 (O₃, CO, NO, NO₂, and SO₂) were simultaneously measured by two sets of instruments, and good agreement was achieved
91 within the uncertainty. VOCs species (alkanes, alkenes, aromatics, isoprene, and oxygenated VOCs (OVOCs)) were measured
92 using a gas chromatograph following a mass spectrometer (GC-MS). In addition, HONO and HCHO were measured as well.
93 Table S1 in the Supplementary Information presents the experimental details of the meteorological and chemical parameters
94 during this campaign.

95 **2.2 The OH and HO₂ measurements**

96 The OH and HO₂ radicals were measured by PKU-LIF based on the fluorescence assay by gas expansion (FAGE) technique.
97 The principle has been reported in previous studies, and only a brief description of the instrument is presented here. Further
98 detailed information on the instrument can be found in previous studies (Heard and Pilling, 2003;Fuchs et al., 2008;Holland
99 et al., 1995;Hofzumahaus et al., 1996;Fuchs et al., 2011).

100 In principle, OH resonance fluorescence is released in the OH excitation by a 308 nm pulsed laser, and then OH radicals are
101 detected directly. HO₂ radicals are converted into OH via NO, and then they are detected. The system contains a laser module
102 and a detection module. Ambient air was drawn into two independent, parallel, low-pressure (3.5 mBar) cells through two
103 parallel nozzles with 0.4 mm diameter pinhole. The OH radicals are excited into resonance fluorescence in the OH detection
104 cell and detected by micro-channel plate detectors (MCP). In the HO₂ detection cell, NO is injected and converts HO₂ to OH
105 radicals, and then OH radicals are excited by the laser and release resonance fluorescence. Besides, an OH reference cell in
106 which a large OH concentration is generated by pyrolysis of water vapor on a hot filament is applied to automatically correct
107 the laser wavelength.

108 Owing to the failure of the reference cell in this campaign, the NO mixing ratios injected into the HO₂ detection cell were
109 set to be higher than that in other campaigns in China because the HO₂ cell needed to be used as a reference cell to correct
110 laser wavelength. In this campaign, NO mixing ratios were switched between 25 ppm (low NO mode) and 50 ppm (high NO
111 mode). We calculated the HO₂-to-OH conversion efficiencies under the two different NO concentrations by calibrating the
112 PKU-LIF system. HO₂-to-OH conversion efficiencies in low NO mode ranged within 80%-95%, while those in high NO mode
113 reached 100%, demonstrating that the high NO concentration is sufficient to achieve the complete HO₂-to-OH conversion and
114 thus the HO₂ measurement was affected by RO₂ radicals. Prior studies have reported the relative detection sensitivities (α_{RO_2})
115 for the major RO₂ species, mainly from alkenes, isoprene and aromatics. Fuchs et al. (2011) reported that the relative RO₂
116 detection sensitivities are approximately constant when the NO concentration is so high that HO₂ conversion in the detection
117 is nearly complete. Thus, when the HO₂-to-OH conversion efficiencies reach 100%, the relative RO₂ detection sensitivities

118 reported by Fuchs et al. (2011) and Lu et al. (2012) can be used for the correction of HO₂ concentrations (Fuchs et al., 2011;Lu
119 et al., 2012;Lu et al., 2013). Herein, only the HO₂ observations in high NO mode were chosen and they were denoted as [HO₂*],
120 which was the sum of the true HO₂ concentration and a systematic bias from the mixture of RO₂ species *i* which were detected
121 with different relative sensitivities $\alpha_{RO_2}^i$, as shown in Eq. (1) (Lu et al., 2012). The true HO₂ concentration was difficult to be
122 calculated because the observed concentrations of RO₂ and their speciation were not available. Herein, we simulated the HO₂
123 and HO₂* concentrations by the model, and the RO₂ interference yields which were used for correction were the modeled
124 values reported by Lu et al. (2012) in the PRIDE-PRD2006 campaign in which the HO₂-to-OH conversion efficiencies also
125 reached 100% due to the injection of pure NO in the HO₂ detection cell. The interference from RO₂ radicals was estimated to
126 be the difference between the modeled HO₂ and HO₂* concentrations. Overall, the measurement uncertainties of OH and HO₂*
127 radicals were 11% and 15%, respectively, as shown in Table S1 in the Supplementary Information.

$$128 \quad [HO_2^*] = [HO_2] + \sum(\alpha_{RO_2}^i \times [RO_2]_i) \quad (1)$$

129 Additionally, prior studies reported that OH measurement might be affected by the potential interference, when the sampled
130 air contains ozone, alkenes and BVOCs (Mao et al., 2012;Fuchs et al., 2016;Novelli et al., 2014), indicating the environmental
131 conditions are important to the production of interference. The pre-injector is usually used to test the potential OH interference,
132 and has been applied to our PKU-LIF system to quantify the possible interferences for several campaigns, including the
133 campaigns conducted at the Wangdu, Heshan, Huairou, Taizhou and Chengdu sites (Tan et al., 2017;Tan et al., 2019;Tan et al.,
134 2018;Yang et al., 2021;Ma et al., 2022b). No significant internal interference was found in the prior studies, demonstrating the
135 accuracy of the PKU-LIF system has been determined for several times. Moreover, to further explore the potential interference
136 in this campaign, we compared the major environmental conditions, especially O₃, alkenes and isoprene, between Shenzhen
137 and Wangdu sites, as shown in the Supplementary Information. The results indicated that the environmental condition in
138 Shenzhen was less conducive to generating interference than that in Wangdu, and the details were presented in the
139 Supplementary Information. Besides the environmental conditions, the prior studies reported that the product of the reaction
140 of RO₂ with OH, trioxides (ROOOH), might lead to an OH interference signal. The reactions of RO₂ radicals with OH radicals
141 might be competitive with other sinks for RO₂ radicals (Fittschen, 2019;Fittschen et al., 2019;Berndt et al., 2022). Fittschen et
142 al. (2019) reported that the OH interference signals might come from the ROOOH heterogeneous decomposition on the walls
143 of the FAGE cell or the entrance nozzle, but they also noted that the ROOOH interference is highly dependent on the design
144 and measurement conditions of different FAGE instruments. Therefore, we integrated the reactions of the ROOOH production
145 and destruction into the base model herein, with the ROOOH production rate constant of $1.5 \times 10^{-10} \text{ cm}^3 \text{ s}^{-1}$ and the destruction
146 rate constant of 10^{-4} s^{-1} (the details are presented in the Supplementary Information) (Fittschen et al., 2019). Figure. S1 (a)
147 presents the modeled ROOOH concentrations during this campaign, with a maximum of about $4.4 \times 10^9 \text{ cm}^{-3}$. The correlation
148 of the modeled ROOOH concentrations and the ratios of OH observations to OH simulations, and the correlation of the

149 modeled ROOOH concentrations and the difference between OH observations and simulations both demonstrated that no
150 significant relevance between ROOOH and the underestimation of OH radicals, as shown in Fig. S1 (b-c). Additionally, the
151 ROOOH values modeled in our another campaign (Taizhou, 2018) were comparable to or even slightly higher than the
152 simulations in this study, and the chemical modulation tests in Taizhou confirmed the ROOOH is not a significant OH
153 interference in our PKU-LIF system (Ma et al., 2022b). Overall, the OH interference during this campaign was negligible
154 according to the analysis of the behavior of PKU-LIF system in previous campaigns, the comparison of environmental
155 conditions between this campaign and Wangdu campaign, and the exploration of the impact of ROOOH on the discrepancy of
156 OH observations and simulations. However, we should acknowledge that the unmeasured interference might have an effect on
157 radical measurement. More precise chemical modulation tests are needed in the future

158

159 **2.3 Closure experiment**

160 As an effective tool to explore the atmospheric radical chemistry, the radical closure experiment can investigate the state-of-
161 the-art chemical mechanism because of the extremely short lifetime of radicals (Stone et al., 2012; Lu et al., 2019). A zero-
162 dimensional box model was used to conduct the radical closure experiment, and the overall framework was reported by Lu et
163 al. (2019). In this work, we conducted the radical closure experiment based on the Regional Atmospheric Chemical Mechanism
164 updated with the latest isoprene chemistry (RACM2-LIM1), as Tan et al. (2017) described in detail. The model was constrained
165 by the measured meteorological, photolysis frequency, and the critical chemical parameters (CO, NO, NO₂, VOCs, *etc.*). The
166 H₂ and CH₄ mixing ratios were set to 550 ppb and 1900 ppb, respectively. The model was operated in time-dependent mode
167 with a 5-min time resolution, and a 2-d spin-up time was to make the unconstrained species approach the steady state relative
168 to the constrained species.

169 As Lu et al. (2012) described, there are two types of radical closure experiment. One is the comparison of observed and
170 modeled radical concentrations, and the other is the comparison of radical production and destruction rates. The most
171 significant difference between the above is that the latter is conducted with the observed radical concentrations and k_{OH}
172 constrained. The comparison of radical production and destruction rates, which is also called radical experimental budget, can
173 test the accuracy of the state-of-the-art chemistry mechanisms based on the equivalent relationship between the radical
174 production and destruction rates. The production rates of OH, HO₂, and RO₂ radicals are quantified from all the known sources.
175 The destruction rates of HO₂ and RO₂ radicals are the sum of the known sinks, while the OH destruction rate can be directly
176 calculated as the product of the observed OH concentrations and the observed k_{OH} (Tan et al., 2019; Yang et al., 2021). The OH
177 destruction rate is the total sinks of OH radicals because of the direct k_{OH} observation, and thus the discrepancy between the
178 OH destruction and production rates denotes the missing OH sources. The detailed reactions and the reaction rate constants
179 related to OH, HO₂, and RO₂ radicals can be found in Tan et al. (2019) and Yang et al. (2021).

180 2.4 AOC evaluation

181 The life time of the trace gases is controlled not only by the oxidant concentration but also by its second-order rate constant,
182 so the atmospheric oxidation capacity (AOC) proposed by Geyer et al. (2001) is most suitable to evaluate the relative
183 importance of each oxidant (Elshorbany et al., 2009). AOC is the core driving force of complex air pollution, and determines
184 the removal rate of trace gases and the production rates of secondary pollutants (Liu et al., 2021). As an effective indicator for
185 atmospheric oxidation intensity, the evaluation of AOC can provide crucial information on the atmospheric composition of
186 harmful and climate forcing species (Elshorbany et al., 2009). AOC is defined as the sum of the respective oxidation rates of
187 the pollutants via reactions with oxidants (Elshorbany et al., 2009;Geyer et al., 2001;Zhu et al., 2020). According to the
188 definition of AOC, it can be calculated by the Eq. (2).

$$189 \text{AOC} = \sum_i k_{Y_i} [Y_i] [X] \quad (2)$$

190 where Y_i are the pollutants (CO, CH₄, and VOCs), X are the main atmospheric oxidants (OH, O₃, NO₃), and k_{Y_i} is the bi-
191 molecular rate constant for the reaction of Y_i with X . AOC includes all combination of pollutants Y and oxidants X . The
192 higher AOC, the higher removal rate of the atmospheric pollutants, and thus the higher production rate of secondary pollutants
193 (Yang et al., 2020b). Simultaneous measurements of OH and the key trace gases are available in the study. NO₃ concentration
194 could be simulated by the box model with the observed parameters constrained.

195 3. Results

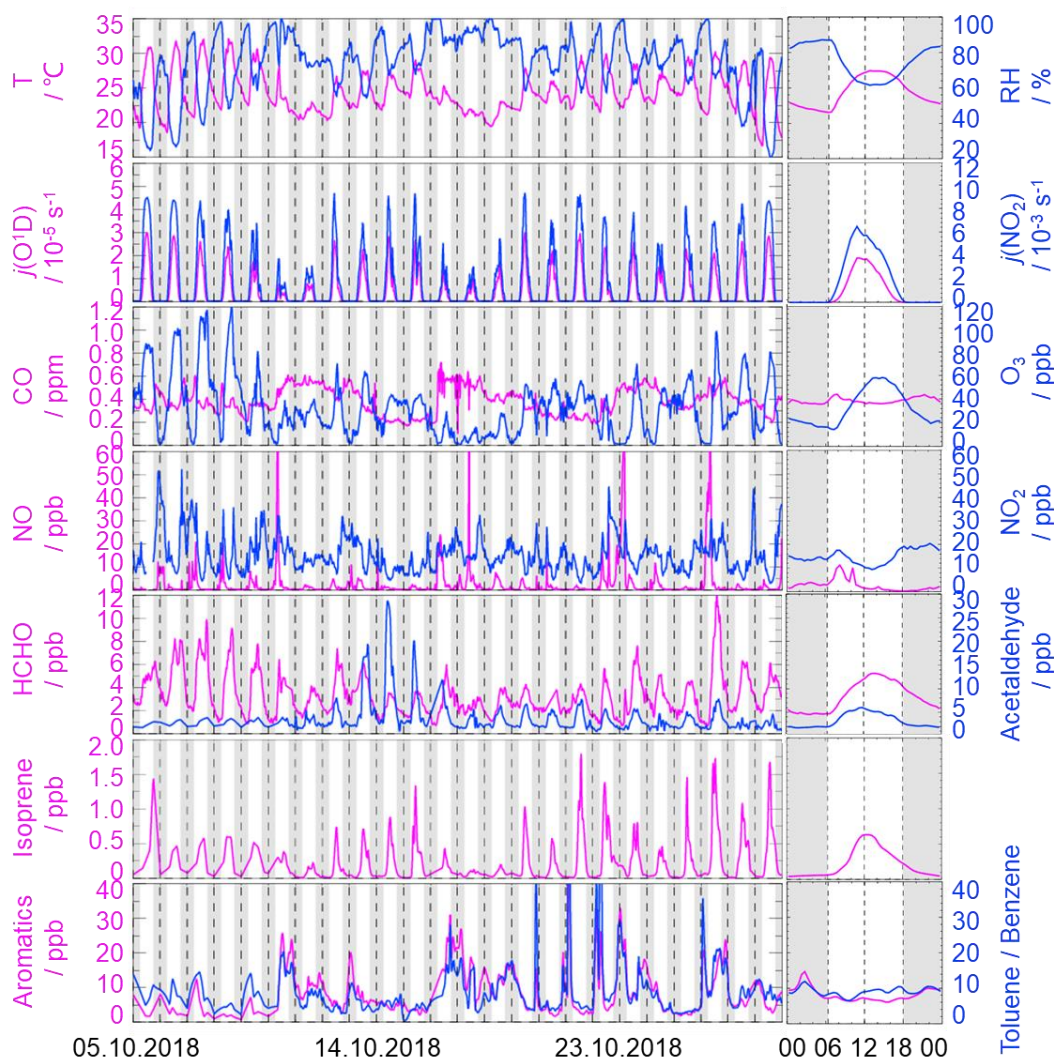
196 3.1 Meteorological and chemical conditions

197 Figure 2 gives an overview of the meteorological and chemical parameters from 05 October to 28 October 2018, when OH
198 and HO₂ radicals were measured. The diurnal variations of the temperature (T), relative humidity (RH), $j(\text{O}^1\text{D})$, and $j(\text{NO}_2)$
199 followed a regular pattern from day to day. The overall meteorological conditions were characterized by high temperature
200 (about 20~30 °C), high relative humidity (60~80%), and intensive radiation with $j(\text{O}^1\text{D})$ up to $2.0 \times 10^{-5} \text{ s}^{-1}$ and $j(\text{NO}_2)$ up to
201 $6.0 \times 10^{-3} \text{ s}^{-1}$. The relative humidity and photolysis-frequency in this autumn campaign were similar to those in the summer
202 campaign conducted in Chengdu (Yang et al., 2021). The temperature in this campaign was lower than that in Chengdu, but
203 similar to that in the autumn campaign in Heshan located in PRD as well (Tan et al., 2019;Yang et al., 2021).

204 The concentration of CO showed a weak diurnal variation, indicating there was the non-obvious accumulation of
205 anthropogenic emissions on a regional scale. NO concentration peaked at 12 ppb during morning rush hour when the traffic
206 emission was severe, and thereafter, O₃ concentration started to increase with the decreasing of NO concentration. The maxima
207 of O₃ hourly concentration were high up to 120 ppb. According to the updated National Ambient Air Quality Standard of China
208 (GB3095-2012), O₃ concentration exceeded the Class-II limit values (hourly averaged limit 93 ppb) on several days (6, 7, 8,
209 and 26 October) when the environmental condition was characterized by high temperature and low relative humidity. NO₂

210 concentration was high at night because of the titration effect of O₃ with NO.

211 Along with the high O₃ concentration on 6, 7, 8, and 26 October, high HCHO concentration was also recorded during the
212 corresponding periods, indicating HCHO was mainly produced as secondary pollutants because of the active photochemistry
213 in this campaign. Isoprene, which is mostly derived from biogenic emissions and mainly affected by temperature, peaked
214 around noontime. Tan et al. (2019) reported the median concentration of HCHO and isoprene concentrations were 6.8 ppb and
215 0.6 ppb during 12:00-18:00 at Heshan site. Similarly, the median concentration of HCHO and isoprene concentrations in this
216 study were 4.9 ppb and 0.4 ppb during the corresponding periods, respectively. As a proxy for traffic intensity, the toluene to
217 benzene ratio (T/B), which is below 2, means the traffic emissions are the major sources of VOCs (Brocco et al., 1997). In this
218 campaign, the T/B gradually dropped from 07:00 until it reached the minimum value at 09:00, indicating traffic emission
219 contributed more to VOCs during morning rush hour than during other periods. However, the T/B values, which varied within
220 a range of 7-12, were above 2, and thus VOCs emission during this campaign was mainly from other sectors such as those
221 involving solvent evaporation.



222
223 **Figure 2: Timeseries and diurnal profiles of the observed meteorological and chemical parameters in the STORM campaign. The**
224 **grey areas denote nighttime.**

225 Moreover, we compared the environmental conditions between the Backgarden (rural site), Heshan (suburban site), and
226 Shenzhen (urban site) campaigns conducted in PRD in Table S3 in the Supplementary Information. No significant discrepancy
227 in temperature was found in the Shenzhen and Heshan campaigns, which were both conducted in autumn. The temperature in
228 the Backgarden campaign conducted in summer was higher than those in Shenzhen and Heshan. The relative humidity in
229 Shenzhen and Backgarden was higher than that in Heshan. Compared to the chemical conditions in the Heshan campaign
230 conducted in autumn as well, the concentrations of CO, NO, NO₂, HONO, alkenes, aromatics, and HCHO in Shenzhen were
231 lower, which might be because there were no significant local pollution sources nearby at the Shenzhen site although it was
232 an urban site. However, the concentration of O₃ which is the typical secondary pollutant in Shenzhen was higher than that in
233 Heshan. Compared to the environmental conditions in Heshan, the higher O₃ concentration in Shenzhen might benefit from
234 the weather condition which was characterized by the stronger solar radiation and slightly higher temperatures.

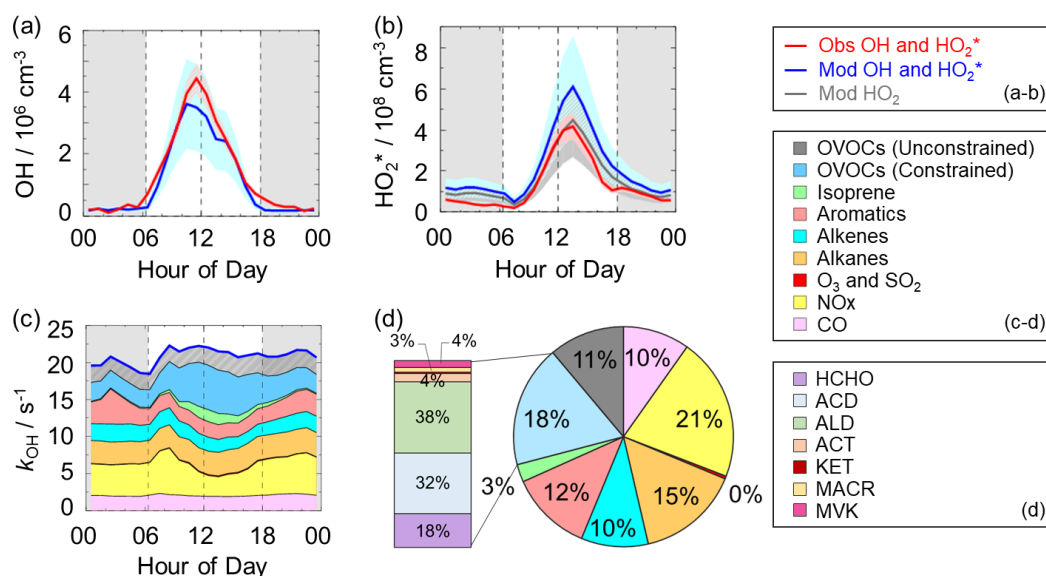
235 3.2 Observed and modeled OH and HO₂ radicals

236 The OH and HO₂ radicals were measured during 05-28 October 2018. The timeseries of the observed and modeled HOx
237 concentrations are displayed in Fig. S2 (a-b) in the Supplementary Information. Data gaps were caused by the rain, calibration,
238 and maintenance. The daily maxima of the observed OH and HO₂^{*} concentrations varied in the range of (2-9) × 10⁶ cm⁻³ and
239 (2-14) × 10⁸ cm⁻³, respectively. As in previous campaigns, the largest OH concentrations appeared around noontime and
240 showed a high correlation with *j*(O¹D), a proxy for the solar UV radiation driving much of the primary radical production (Tan
241 et al., 2019).

242 Figure 3 (a-b) shows the diurnal profiles of the observed and modeled HOx concentrations. The HOx radicals showed similar
243 diurnal behavior to those reported in other campaigns (Ma et al., 2019a; Tan et al., 2017; Tan et al., 2019; Tan et al., 2018; Yang
244 et al., 2021). The observed OH and HO₂^{*} concentrations reached a maximum around 12:00 and 13:30, respectively. The
245 diurnal maxima of the observed and modeled OH concentrations were 4.5 × 10⁶ cm⁻³ and 3.5 × 10⁶ cm⁻³. Compared to the
246 other campaigns conducted in PRD (Backgarden and Heshan), the diurnal maximum of the observed OH concentration in
247 Shenzhen was equal to that observed in Heshan, and much lower than that observed in Backgarden where the observed OH
248 concentration was nearly 15 × 10⁶ cm⁻³ (Hofzumahaus et al., 2009; Tan et al., 2019). The higher OH concentration at
249 Backgarden site was closely correlated to the stronger solar radiation, as shown in Table S3 in the Supplementary Information.
250 The diurnal observed and modeled OH concentrations agreed within their 1-σ uncertainties of measurement and simulation
251 (11% and 40%). However, when the NO mixing ratio (Fig. 2) dropped from 10:00 gradually, a systematic difference existed,
252 with the observed OH concentration being about 1 × 10⁶ cm⁻³ higher than the modeled OH concentration. The OH
253 concentrations observed in the environments with low NO levels were underestimated by the state-of-the-art models at
254 Backgarden (summer) and Heshan (autumn) sites in PRD as well, and the OH underestimation was identified to be universal
255 at low NO conditions in China (Lu et al., 2013; Lu et al., 2012; Ma et al., 2019a; Tan et al., 2017; Yang et al., 2021; Ma et al.,

256 2022b). The reason on OH underestimation was further discussed in Section 4.1.

257



258

259 **Figure 3:** (a-b) The diurnal profiles of the observed and modeled OH, HO_2^* and HO_2 concentrations. (c) The diurnal profiles of the
260 modeled k_{OH} . (d) The composition of the modeled k_{OH} . The red areas in (a-b) denote 1- σ uncertainties of the observed OH and HO_2^*
261 concentrations. The blue areas in (a-b) denote 1- σ uncertainties of the modeled OH and HO_2^* concentrations, and the dark grey
262 area in (b) denotes 1- σ uncertainties of the modeled HO_2 concentrations. The grey areas in (a-c) denote nighttime. ACD denotes
263 acetaldehydes. ALD denotes the C3 and higher aldehydes. ACT and KET denote acetone and ketones. MACR and MVK denote
264 methacrolein and methyl vinyl ketone.

265 The diurnal maximum of the observed HO_2^* , the modeled HO_2^* and the modeled HO_2 concentrations were $4.2 \times 10^8 \text{ cm}^{-3}$,
266 $6.1 \times 10^8 \text{ cm}^{-3}$, and $4.4 \times 10^8 \text{ cm}^{-3}$, respectively. The difference between the modeled HO_2^* and HO_2 concentrations can be
267 considered a modeled HO_2 interference from RO_2 (Lu et al., 2012). The RO_2 interference was small in the morning, while it
268 became larger in the afternoon. It ranged within 23%-28% during the daytime (08:00-17:00), which was comparable with
269 those at Backgarden and Yufa sites in China, Borneo rainforest in Malaysia (OP3 campaign, aircraft), and UK (RONOCO
270 campaign, aircraft) (Lu et al., 2012; Lu et al., 2013; Jones et al., 2011; Stone et al., 2014). The observed HO_2^* was overestimated
271 by the model, indicating the HO_2 heterogeneous uptake might have a significant impact during this campaign. The diurnal
272 maximum of HO_2^* concentration observed in Shenzhen was much lower than those observed at the Yufa and Backgarden sites
273 (Hofzumahaus et al., 2009; Lu et al., 2012; Lu et al., 2013). The high modeled HO_2/OH ratio around noontime (11:00-15:00),
274 which was about 138, was found in this campaign, which was higher than those at the Backgarden and Chengdu sites (Yang
275 et al., 2021; Hofzumahaus et al., 2009). High HO_2/OH ratio is normally found only in clean air at low NO_x ($= \text{NO} + \text{NO}_2$)
276 concentrations (Hofzumahaus et al., 2009; Stevens et al., 1997). As an indicator that can reflect the interconversion reaction
277 between HO_2 and OH, the conversion efficiency in this campaign was slightly slower than those at the Backgarden and
278 Chengdu sites.

279 3.3 OH reactivity

280 k_{OH} is the pseudo-first-order loss rate coefficient of OH radicals, and it is equivalent to the reciprocal OH lifetime (Fuchs et
281 al., 2017; Lou et al., 2010; Yang et al., 2019). In this campaign, k_{OH} was measured only for several days (05-19 October 2018)
282 by the LIP-LIF system, which has been reported in the previous study (Liu et al., 2019). The timeseries of the observed and
283 modeled k_{OH} during 05-19 October 2018 are presented in Fig. S3 in the Supplementary Information. A good agreement between
284 the observed k_{OH} and modeled k_{OH} within the uncertainties was achieved, and thus the model can be believed to reproduce the
285 observed k_{OH} values within the whole campaign. Moreover, to reflect the k_{OH} in the whole campaign, the modeled values were
286 shown in the k_{OH} diurnal profiles (Fig. 3 (c)) and k_{OH} timeseries (Fig. S2 (c)) during 05-28 October 2018. The modeled k_{OH}
287 showed a weak diurnal variation and varied from 18 s^{-1} to 22 s^{-1} . Compared to the k_{OH} variation in Shenzhen, the k_{OH} observed
288 at Backgarden and Heshan sites in PRD showed a stronger diurnal variation, with a minimum value at around noontime and a
289 maximum value at daybreak. Additionally, the k_{OH} values in this campaign were lower than those at Backgarden ($20\text{-}50 \text{ s}^{-1}$)
290 and Heshan ($22\text{-}32 \text{ s}^{-1}$) sites (Lou et al., 2010; Tan et al., 2019). Similar with the good agreement between the observed and
291 modeled k_{OH} during the several days in Shenzhen, the observed k_{OH} in Backgarden was matched well with the modeled k_{OH}
292 which has included the OVOCs reactivity. In terms of the k_{OH} in Heshan, Tan et al. (2019) reported that only half of the
293 observed k_{OH} was explained by the calculated k_{OH} which was calculated from the measured trace gas concentrations. The
294 missing k_{OH} in Heshan was likely caused by unmeasured VOCs, demonstrating the necessary to measure more abundant VOCs
295 species, especially OVOCs species.

296 As shown in Fig. 3 (d), we presented the composition of modeled k_{OH} . The inorganic compounds contributed approximately
297 31% to k_{OH} , in which the CO and NOx reactivity accounted for 10% and 21%, respectively. The NOx reactivity was displayed
298 versus time, with a maximum during the morning peak. The peak concentration during the morning peak was associated with
299 traffic emissions.

300 Compared with the inorganic reactivity, the larger fraction of k_{OH} came from the VOCs group, with a contribution of 69%
301 to k_{OH} . The contribution of alkanes, alkenes, and aromatics were 15%, 10%, and 12%, respectively. The isoprene reactivity
302 related to temperature was mainly concentrated during the daytime, whereas the aromatics reactivity at night was higher. As
303 for the OVOCs species, we measured several OVOCs species, including HCHO, acetaldehydes (ACD) and higher aldehydes
304 (ALD), acetone (ACT), ketones (KET) and isoprene oxidation products (methacrolein (MACR) and methyl vinyl ketone
305 (MVK)), and thus we constrained these species in the model. The constrained OVOCs species accounted for 18% in the total
306 k_{OH} , where HCHO, ACD, and ALD were the major contributors, with contributions of 18%, 32%, and 38% to the constrained
307 OVOCs, respectively. The contribution of aldehydes in this study (16%) was larger than that in Beijing (Whalley et al., 2021)
308 and smaller with that in Wangdu (Fuchs et al., 2017). The remaining reactivity was attributed to the unconstrained OVOCs
309 reactivity, which came from the model-generated intermediate species (glyoxal, methylglyoxal, methyl ethyl ketone, methanol,

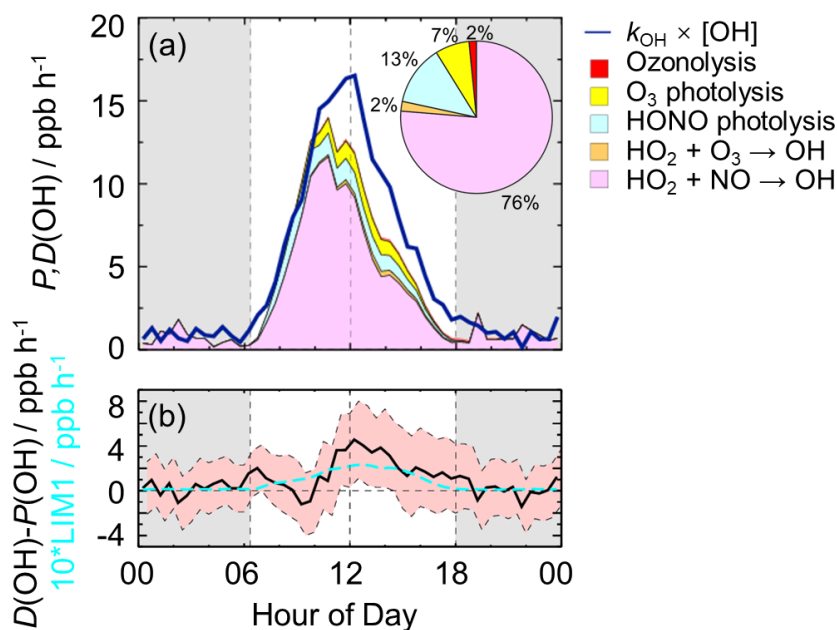
etc.), with a contribution of 11% to the total k_{OH} . Large fraction of OVOCs reactivities in k_{OH} was also found in some previous studies (Lou et al., 2010; Lu et al., 2013; Fuchs et al., 2017; Whalley et al., 2021). About 50% of k_{OH} was explained by OVOCs at Backgarden site, and HCHO, ACD and ALD, and oxygenated isoprene products were the most important OH reactants in OVOCs, with a contribution of 30-40%, and other 10-20% came from other oxygenated compounds (ketones, dicarbonyl compounds, alcohols, hydroperoxides, nitrates etc.) (Lou et al., 2010). HCHO, ACD, MVK, MVCR and glyoxal accounted for one-third of the total k_{OH} at Wangdu site (Fuchs et al., 2017). The large unconstrained OVOCs reactivity indicated it is necessary to measure more VOCs species in the future.

4. Discussion

4.1 Radical closure experiment

In this study, we conducted OH radical closure experiment which is called OH experimental budget as well. As discussed in Section 3.3, it is believed that the model can reproduce the observed k_{OH} . Herein, to conduct the OH experiment budget in the whole campaign, we used the modeled k_{OH} to calculate the OH destruction rate because the k_{OH} was only measured on several days. The diurnal profiles of OH production and destruction rates, and the compositions of OH production rate were displayed in Fig. 4, with maxima of 14 ppb h⁻¹ and 17 ppb h⁻¹ around noontime, respectively. The OH production rate from known sources is quantified from the primary sources (photolysis of HONO, photolysis of O₃, ozonolysis of alkenes) and secondary sources (dominated by HO₂ + NO, and HO₂ + O₃). The primary and secondary sources accounted for 78% and 22% of the total calculated production rate, respectively. Similar with the prior studies, the largest fraction of OH production rate came from HO₂ + NO, with a contribution up to 76% of the known OH production rate. As the major primary OH sources, the HONO and O₃ photolysis contributed 13% and 7% to the total calculated OH production rate, respectively.

The OH production rate matched well with the destruction rate only in the early morning to about 10:00. Thereafter, the OH destruction rate was larger than the production rate, which could explain the underestimation of OH concentration by the model. As shown in Fig. 4 (b), the discrepancy between the OH production and destruction rates at around 11:00-15:00, which was approximately of (3.1~4.6) ppb h⁻¹, cannot be explained by the combined experimental uncertainties. The discrepancy was attributed to the missing OH sources because k_{OH} was constrained in this study. The biggest additional OH source was approximately 4.6 ppb h⁻¹, which occurred at about 12:00, when the OH production and destruction rates were 11.9 ppb h⁻¹ and 16.5 ppb h⁻¹, respectively. The unknown OH source accounted for about one third of the total OH production rate, indicating the exploration of missing OH source was significant to study the radical chemistry. It is noted that the OH production rate was overestimated because we used HO₂^{*} concentrations instead of HO₂ concentrations here. Thus, the missing OH source was the lower limit here, demonstrating more unknown OH sources need to be further explored. Details on unknown OH sources are given below (Sect. 4.2).



341

342 **Figure 4: (a) The diurnal profiles of OH production and destruction rates and the proportions of different known sources in the**
 343 **calculated production rate during the daytime. The blue line denotes the OH destruction rate, and the colored areas denote the**
 344 **calculated OH production rates from the known sources. (b) The missing OH source which was the discrepancy between the OH**
 345 **destruction and production rates, and the OH production rate which was ten times the production rate derived from LIM1**
 346 **mechanism. The red shaded areas denote the combined uncertainty from the experimental errors of the measured quantities (Table**
 347 **S1) and the reaction rate coefficients. The grey areas denote nighttime.**

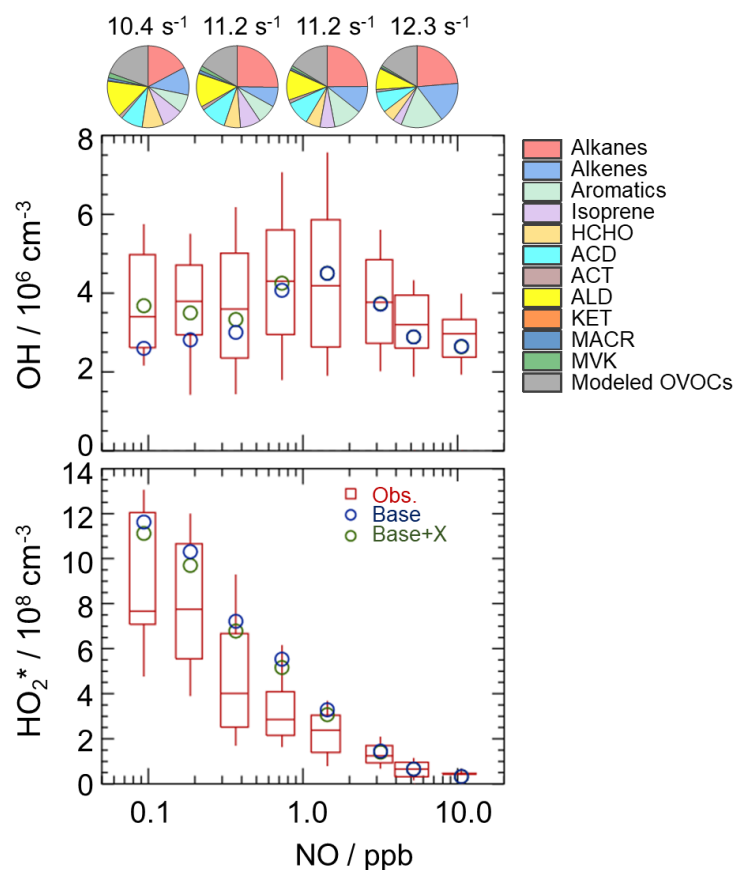
348

349 4.2 Radical chemistry in low NO regime

350 4.2.1 Influencing factors of OH underestimation

351 As analyzed in Sect. 4.1, the underestimation of OH concentration was attributable to the missing OH source. It is necessary
 352 to explore the influencing factor for gaining further insight into the missing source. Scientists reported that more significant
 353 OH underestimation would appear with the decreasing NO concentration and increasing isoprene concentration (Lu et al.,
 354 2012;Ren et al., 2008;Hofzumahaus et al., 2009;Lelieveld et al., 2008;Whalley et al., 2011;Tan et al., 2017;Yang et al., 2021).
 355 Herein, we further explored the effect of NO concentration on missing OH source. The NO dependence on observed and
 356 modeled HOx concentrations and the NO dependence on HOx observed-to-modeled ratios were illustrated in Fig. 5 and Fig.
 357 S4. The OH concentrations were normalized by the averaged $j(\text{O}^1\text{D})$ to eliminate the influence of radiation on radicals. The
 358 OH concentration showed an increasing trend with the increase of NO concentrations in low NO regime (below 1 ppb) due to
 359 the increased OH radicals from propagation via peroxy reactions with NO, and then decreased with the increase of NO
 360 concentrations in high NO regime (above 1 ppb) due to the OH loss by the reactions via NO_2 (Ehhalt, 1999). The base model
 361 can reproduce the observed OH concentration in high NO regime, while underestimate OH concentration in low NO regime.

362 As for HO_2^* radicals, the observed and modeled HO_2^* concentrations decreased with the increase of NO concentrations. The
 363 model overestimated the observations, indicating that the heterogeneous uptake might make a significant role in HO_2 sinks in
 364 this campaign. Overall, NOx plays a crucial role in radical chemistry due to their impact on radical propagation and termination
 365 reactions.



366
 367 **Figure 5: NO dependence on OH and HO_2^* radicals. The red box-whisker plots give the 10%, 25%, median, 75%, and 90% of the**
 368 **HOx observations. The blue circles show the median values of the HOx simulations by the base model, and the green circles show**
 369 **the HOx simulations by the model with X mechanism. Total VOCs reactivity and their organic speciation are presented by pie charts**
 370 **at the different NO intervals at the top. Only daytime values and NO concentration above the detection limit of the instrument were**
 371 **chosen. ACD and ACT denote acetaldehyde and acetone, respectively. ALD denotes the C3 and higher aldehydes. KET denotes**
 372 **ketones. MACR and MVK, which are both the isoprene oxidation products, denote methacrolein and methyl vinyl ketone,**
 373 **respectively.**

374 To further explore the influencing factors of OH underestimation, we presented the speciation VOCs reactivity under the
 375 different NO intervals, as shown in Fig. 5 and Table S4 in the Supplementary Information. The isoprene reactivity and total
 376 OVOCs reactivity (the sum of HCHO, ACD, ACT, ALD, KET, MACR, MVK and the modeled OVOCs) increased with the
 377 decrease of NO concentrations, while the anthropogenic VOCs reactivity (alkanes, alkenes and aromatics) was higher in high
 378 NO regime. Additionally, the O_3 concentration in low NO regime was significantly higher than those in high NO regime, and
 379 the temperature was slightly higher in low NO regime, demonstrating the photochemistry was more active in low NO regime
 380 in this campaign. Overall, the photochemistry and composition of VOCs reactivity, especially the isoprene and OVOCs species
 381 (mainly HCHO, ACD, ALD and the modeled OVOCs), might closely impact the missing OH sources.

382 4.2.2 Quantification of missing OH sources

383 Hofzumahaus et al. (2009) proposed an existence of a pathway for the regeneration of OH independent of NO, including the
384 conversions of $\text{RO}_2 \rightarrow \text{HO}_2$ and $\text{HO}_2 \rightarrow \text{OH}$ by a numerical species called X. With a retrospective analysis, the unclassical
385 OH recycling pathway was identified to be universal at low NO conditions in China. The amount of X varies with
386 environmental conditions, and the X concentrations were 0.85 ppb, 0.4 ppb, 0.1 ppb, 0.4 ppb, 0.1 and 0.25 ppb at Backgarden,
387 Yufa, Wangdu, Heshan, Taizhou, and Chengdu sites (Hofzumahaus et al., 2009; Lu et al., 2012; Lu et al., 2013; Tan et al.,
388 2017; Yang et al., 2021; Ma et al., 2022b).

389 In this study, we tested this unclassical X mechanism. Good agreement between observations and simulations of OH radicals
390 was achieved when a constant mixing ratio of 0.1 ppb of X was added into the base model. As shown in Fig. 5, the model with
391 X mechanism agreed with the observed OH concentrations even at low NO conditions. Unclassical OH recycling was identified
392 again in this study. Nevertheless, X is an artificial species that behaves like NO, and thus the nature of X is still unknown to
393 us. Compared to the Shenzhen site, the required X concentration in the Backgarden and Heshan sites in PRD was higher, which
394 might be affected by the different air masses in the three sites. The k_{OH} at Shenzhen site was much lower than those at
395 Backgarden and Heshan sites (Lu et al., 2013), and a weaker diurnal variation of k_{OH} in Shenzhen was observed. Under the
396 influence of the East Asian monsoon, the prevailing wind for PRD area is mostly southerly during the summer months and
397 mostly northerly during the winter months (Fan et al., 2005; Zhang et al., 2008). The Backgarden site is located in Guangzhou,
398 and the Heshan site is located in Jiangmen. The two cities are along the north-south axis, and thus the air masses of the
399 Backgarden and Heshan sites are intimately linked with each other, while the air mass in Shenzhen is more similar to Hongkong
400 (Zhang et al., 2008). Compared to the VOCs reactivity in the air mass at Backgarden and Yufa sites reported by Lu et al. (2013),
401 lower isoprene reactivity and OVOCs reactivity were observed in Shenzhen site. As discussed in Section 4.2.1, the OH
402 underestimation might be closely related to the composition of VOCs reactivity. Therefore, further exploration of this
403 unclassical OH recycling is needed to improve our understanding of radical chemistry, especially the mechanisms related to
404 isoprene and OVOCs.

405 As for the potential influence of isoprene and OVOCs on the missing OH source, RO_2 isomerization reactions have also
406 been shown to be of importance for the atmospheric fate of RO_2 from isoprene (Peeters et al., 2009; Peeters et al., 2014). The
407 latest isoprene isomerization mechanism, which is called LIM1, has been coupled into our current base model. However, LIM1
408 mechanism was not included in the OH experimental budget which was conducted with the observations constrained, as shown
409 in Section 4.1. Herein, we evaluated the contribution of LIM1 mechanism to the missing OH sources, as shown in Fig. 4 (b).
410 LIM1 mechanism can explain approximately 7% of the missing OH sources during 10:00-16:00, when the missing OH
411 production rate and the OH production rate derived from LIM1 mechanism were 2.47 ppb h^{-1} and 0.17 ppb h^{-1} , respectively.

412 Additionally, prior studies also reported that OH regeneration might be achieved from the oxidation of MACR and MVK,

413 which are the major first-generated products of isoprene (Fuchs et al., 2018;Fuchs et al., 2014). As a potential explanation for
 414 the high OH concentration, the impacts of MACR and MVK oxidation were evaluated here. The modification of MACR
 415 oxidation scheme added the H-migration reactions of MACR oxidation products (Fuchs et al., 2014). The modification of
 416 MVK oxidation scheme added the reactions of MVK oxidation products with HO₂ radicals and the H-migration reactions of
 417 MVK oxidation products (Fuchs et al., 2018). As presented in Fig. S5 in the Supplementary Information, no significant of the
 418 MACR and MVK oxidation schemes was found in this campaign.

419 Overall, a large part of missing OH sources was not explained by the isoprene chemistry. In the future, the impact of OVOCs
 420 species which was another potential OH source on missing OH sources need to be further evaluated.

421 4.3 HO₂ heterogeneous uptake

422 The HO₂^{*} overestimation was identified by comparing the observed and modeled HO₂^{*} concentrations in Sect. 3.2 and Sect.
 423 4.2.1. The HO₂ heterogeneous uptake has been proposed to be a potential sink of HO₂ radicals, and thus could influence the
 424 radical chemistry and the formation of secondary pollution, especially in high-aerosol environments (Song et al., 2021;Song
 425 et al., 2022;Tan et al., 2020;Kanaya et al., 2000;Kanaya et al., 2007;Li et al., 2019). The impact of HO₂ uptake chemistry on
 426 radical concentration is different under different environmental conditions (Whalley et al., 2015;Mao et al., 2010;Li et al.,
 427 2019). To evaluate the contribution of HO₂ uptake chemistry to radical concentrations in this study, we coupled HO₂
 428 heterogeneous uptake into the base model (RACM2-LIM1) and conducted three sensitivity experiments, as shown in R1 and
 429 Eq. (3).



$$431 k_{\text{HO}_2+\text{aerosol}} = \frac{\gamma \cdot \text{ASA} \cdot v_{\text{HO}_2}}{4} \quad (3)$$

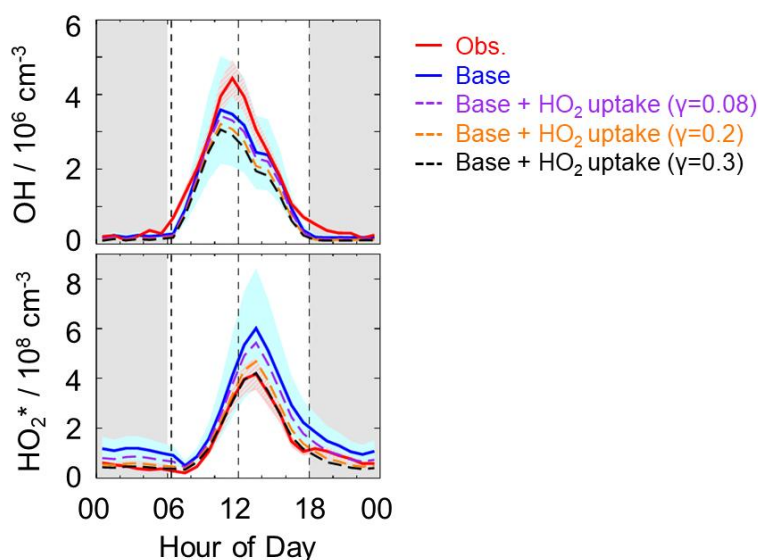
432 where ASA [μm² cm⁻³], which represents the aerosol surface area concentration, can be estimated by multiplying the mass
 433 concentration of PM_{2.5} [μg m⁻³] by 20 here because there were no direct ASA observations in this campaign (Chen et al.,
 434 2019;Wang et al., 2017b). v_{HO_2} , which can be calculated by Eq. (4), refers to the mean molecular velocity of HO₂ with a unit
 435 of cm s⁻¹.

$$436 v_{\text{HO}_2} = \sqrt{\frac{8 \cdot R \cdot T}{0.033 \cdot \pi}} \quad (4)$$

437 where T [K] and R [J mol⁻¹ K⁻¹] denote the ambient temperature and gas constant. γ , the HO₂ effective uptake coefficient,
 438 parameterizes the influence of some processes (Tan et al., 2020). γ varies in the highly uncertain range of 0-1 (Song et al.,
 439 2022), and is the most critical parameter to impact HO₂ uptake chemistry. Only several observations of γ have been reported
 440 (Taketani et al., 2012;Zhou et al., 2021;Zhou et al., 2020). The measured γ at the Mt. Tai site and Mt. Mang site were 0.13-
 441 0.34 and 0.09-0.40, respectively (Taketani et al., 2012). The average value of the measured γ was 0.24 in Kyoto, Japan in the

442 summer of 2018 (Zhou et al., 2020). Zhou et al. (2021) reported the lower-limit values for median and average values of the
443 measured γ were 0.19 and 0.23 ± 0.21 in Yokohama, Japan in the summer of 2019. Additionally, Li et al. (2018) set 0.2 as the
444 value of γ in the model, and Tan et al. (2020) calculated the γ of 0.08 ± 0.13 by the analysis of the measured radical budget in
445 Wangdu.

446 Here, we applied the two γ (0.2 and 0.08), which have been used in the model, to evaluate the impact of HO_2 uptake on
447 radical concentrations, as shown in Fig. 6. The modeled HO_2^* cannot match well with the observations when γ of 0.08 and 0.2
448 was set in the model. As the γ increased to approximately 0.3, good agreement between the modeled and observed HO_2^*
449 concentration was achieved, demonstrating that a significant heterogeneous uptake might exist in this campaign. It should be
450 noted that the HO_2 heterogeneous uptake ($\gamma = 0.3$) reduced the modeled OH concentrations by around 20% compared to the
451 OH simulations in the base model during the daytime (08:00-18:00). Sensitivity tests illustrated that good agreements of OH
452 observations-simulations and HO_2^* observations-simulations were both achieved when the amount of X changed from 0.1 ppb
453 to 0.25 ppb and the HO_2 effective uptake coefficient was 0.3, as shown in Fig. S6 in the Supplementary Information. Compared
454 to the Backgarden and Heshan sites, the amount of X in Shenzhen was still lower despite a significant HO_2 heterogeneous
455 uptake, which might be closely related to the environmental conditions as discussed in Sect. 4.2.

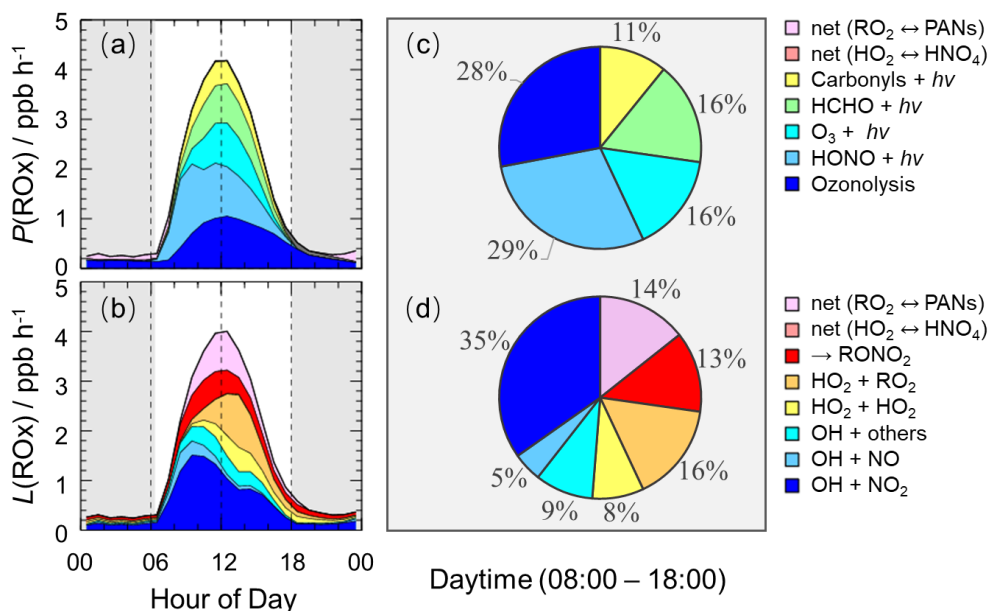


456
457 **Figure 6: The diurnal profiles of the observed and modeled radical concentrations. The red and blue areas denote 1- σ uncertainties**
458 **of measured and simulated radical concentrations by the base model, respectively. The orange, purple and black lines denote the**
459 **simulations by the model which added the HO_2 heterogeneous uptake with different uptake coefficient. The grey areas denote**
460 **nighttime.**

461 It is noted that the estimated strong influence is speculative because of the uncertainties of measurements and simulations.
462 Overall, the γ evaluated in this study was comparable with those observed at the Mt. Tai and Mt. Mang in China, and Kyoto
463 and Yokohama in Japan.

464 **4.4 Sources and sinks of ROx**

465 The detailed analysis of radical sources and sinks was crucial to exploring radical chemistry. The experimental budget for HO₂
 466 and RO₂ radicals could not be conducted because RO₂ was not measured during this campaign. Herein, we showed the
 467 simulated results by the base model. Figure 7 illustrates the diurnal profiles of ROx primary production rate ($P(\text{ROx})$) and
 468 termination rate ($L(\text{ROx})$), and the contributions of different channels during the daytime.



469
 470 **Figure 7: The diurnal profiles of ROx primary production rate (a) and termination rate (b) simulated by the base model, and the**
 471 **contributions of different channels to ROx primary production rate (c) and termination rate (d) during the daytime (08:00-18:00).**
 472 **The grey areas denote nighttime.**

473 The ROx primary production and termination rates were basically in balance for the entire day, with maxima of 4 ppb h^{-1}
 474 around noontime. The ROx primary production rate was similar to those at Heshan (4 ppb h^{-1}) and Wangdu (5 ppb h^{-1}) sites,
 475 but lower than those at Backgarden (11 ppb h^{-1}), Yufa (7 ppb h^{-1}), Taizhou (7 ppb h^{-1}) and Chengdu (7 ppb h^{-1}) sites (Lu et al.,
 476 2013;Lu et al., 2012;Tan et al., 2017;Tan et al., 2019;Yang et al., 2021). During the daytime, the $P(\text{ROx})$ mainly came from
 477 the OH and HO₂ primary production. HONO and O₃ photolysis dominated the OH primary production, and HCHO photolysis
 478 dominated the HO₂ primary production. Thus, $P(\text{ROx})$ was dominated by the photolysis reactions, in which the photolysis of
 479 HONO, O₃, HCHO, and carbonyls accounted for 29%, 16%, 16%, and 11% during the daytime, respectively. In the early
 480 morning, HONO photolysis was the most important primary source of ROx, and the contribution of O₃ photolysis became
 481 progressively larger and was largest at noontime. A large discrepancy between the ratio of HONO photolysis rate to O₃
 482 photolysis rate in summer/autumn and that in winter occurs generally. The vast majority of OH photolysis source is attributed
 483 to HONO photolysis in winter because of the higher HONO concentration and lower O₃ concentration. About half of $L(\text{ROx})$
 484 came from OH termination, which occurred mainly in the morning, and thereafter, radical self-combination gradually became
 485 the major sink of ROx in the afternoon. OH + NO_2 , OH + NO, and OH + others contributed 35%, 5%, and 9% to $L(\text{ROx})$,

486 respectively. HO₂ + HO₂ and HO₂ + RO₂ accounted for 8% and 16% in *L*(RO_x).

487 4.5 AOC evaluation

488 AOC controls the abundance of precursors and the production of secondary pollutants (Yang et al., 2020a; Elshorbany et al.,
489 2009), and thus it is necessary to quantify AOC for understanding photochemical pollution. The AOC has been evaluated in
490 previous studies, as shown in Table 1. Overall, the AOC values in summer are higher than those in autumn and winter, and the
491 values at lower latitudes are higher than those at higher latitudes for the same season. The vast majority of AOC in previous
492 studies are evaluated based on the non-observed radical concentrations.

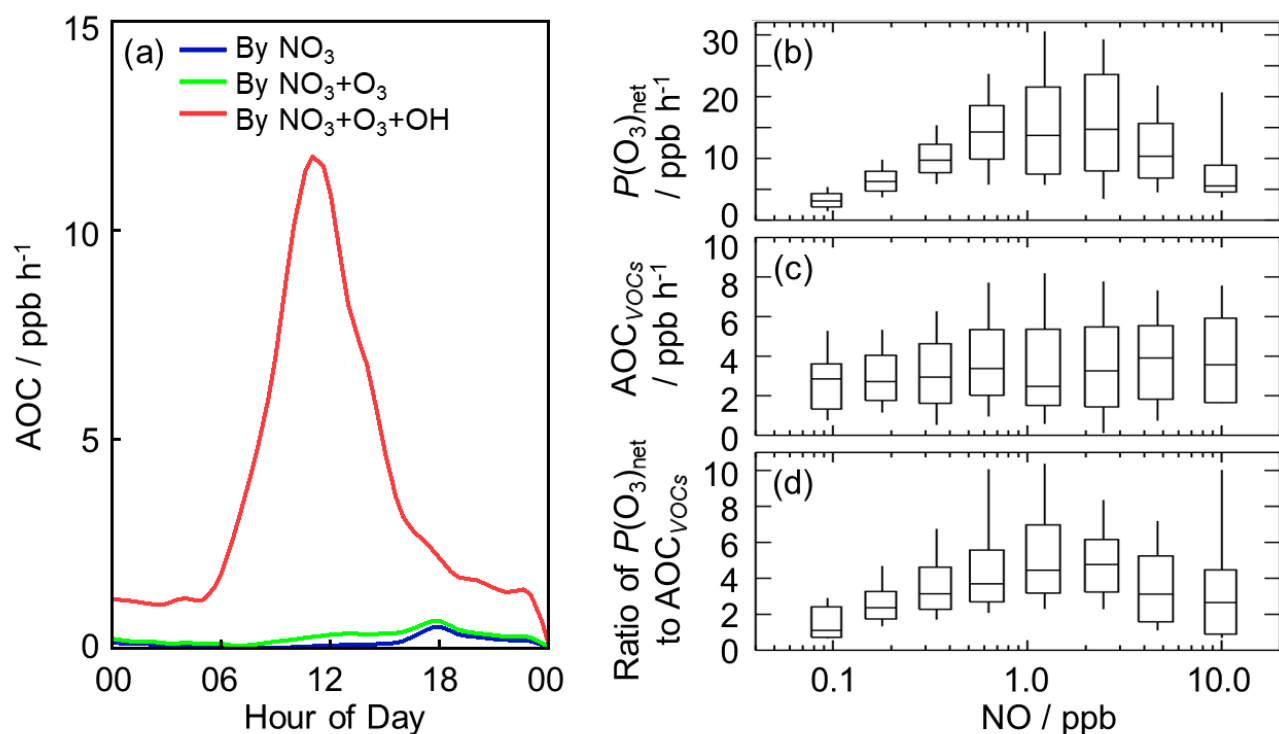
493 **Table 1: Summary of OH concentrations and AOC values reported in previous field campaigns.**

Location	Season, year	Site	Observed or non-observed radicals	of OH molecules cm ⁻³ s ⁻¹	AOC / 10 ⁸	References
Beijing, China	summer, 2018	urban	non-observed values		0.89 ^a	(Liu et al., 2021)
Beijing, China	summer, 2018	suburban	non-observed values		0.85 ^a	(Liu et al., 2021)
Beijing, China	winter, 2018	urban	non-observed values		0.21 ^a	(Liu et al., 2021)
Beijing, China	winter, 2018	suburban	non-observed values		0.16 ^a	(Liu et al., 2021)
Hongkong, China	summer, 2011	suburban	non-observed values		2.04 ^{a,b}	(Xue et al., 2016)
Santiago, Chile	summer, 2005	urban	non-observed values		3.4 ^a	(Elshorbany et al., 2009)
Hong Kong, China	late summer, 2012	coastal	non-observed values		1.4 ^c	(Li et al., 2018)
Hong Kong, China	autumn, 2012	coastal	non-observed values		0.62 ^c	(Li et al., 2018)
Hong Kong, China	winter, 2012	coastal	non-observed values		0.41 ^c	(Li et al., 2018)
Shanghai, China	summer, 2018	urban	non-observed values		1.0 ^c	(Zhu et al., 2020)
Berlin, Germany	summer, 1998	suburban	non-observed values		0.14 ^d	(Geyer et al., 2001)
Xianghe, China	autumn, 2019	suburban	non-observed values		0.49 ^c	(Yang et al., 2020a)
Beijing, China	summer, 2014	urban	non-observed values		1.7 ^a	(Feng et al., 2021)

494 Note that:

495 ^a Peak values in the diurnal profiles; ^b Values on 25 August 2021; ^c Maximum over a period of time; ^d Maximum on some day.

496 Herein, we explored the AOC in Shenzhen based on the observed radical concentrations for the first time. As illustrated in
497 Fig. 8 (a), the diurnal profile of AOC exhibited a unimodal pattern, which was the same as the diurnal profile of OH
498 concentration and *j*(NO₂), with a peak around noontime. The diurnal peak of AOC was 0.75 × 10⁸ molecules cm⁻³ s⁻¹ (11.8 ppb
499 h⁻¹). Comparatively, AOC in this study was comparable to those evaluated in Beijing (summer, 2018) and Hong Kong (autumn,
500 2012) (Li et al., 2018; Liu et al., 2021), but much lower than those evaluated in Hong Kong (summer, 2011) and Santiago



502

503 **Figure 8: (a) The diurnal profiles of AOC in this campaign. (b) NO dependence on $P(O_3)_{net}$ during the daytime. (c) NO dependence**
 504 **on AOC_{VOCs} during the daytime, and AOC_{VOCs} denotes the atmospheric oxidation capacity only from the VOCs oxidation. (d) NO**
 505 **dependence on the ratio of $P(O_3)_{net}$ to AOC_{VOCs} during the daytime. The box-whisker plots in (b-d) give the 10%, 25%, median, 75%,**
 506 **and 90% $P(O_3)_{net}$, AOC_{VOCs} and the ratio of $P(O_3)_{net}$ to AOC_{VOCs} , respectively.**

507 As expected, the dominant contributor to the AOC during this campaign was OH, followed by O_3 and NO_3 . Figure S7 shows
 508 the fractional composition of the total AOC. The OH radical contributed about 95.7% of AOC during the daytime (08:00-
 509 18:00). O_3 , as the second important oxidant, accounted for only 2.9% of AOC during the daytime. The contribution of NO_3 to
 510 AOC during the daytime can be ignored, with a contribution of 1.4%. At night, the contributions of O_3 and NO_3 to AOC were
 511 higher. OH, O_3 and NO_3 accounted for 75.6%, 6.4%, and 18% in the first half of night (18:00-24:00), and they accounted for
 512 87.7%, 5%, and 7.3% in the second half of night (00:00-08:00).

513 As the indicator for secondary pollution, net O_3 production rate, $P(O_3)_{net}$, can be calculated from the O_3 formation rate ($F(O_3)$)
 514 and the loss rate ($L(O_3)$), as shown in Eq. (5-7) (Tan et al., 2017). The diurnal profiles of the speciation $F(O_3)$ and $L(O_3)$ were
 515 shown in Fig. S8 in the Supplementary Information. The diurnal maxima of the modeled $F(O_3)$ and $L(O_3)$ were 18.9 ppb h⁻¹
 516 and 2.8 ppb h⁻¹, with the maximum $P(O_3)_{net}$ of 16.1 ppb h⁻¹ at around 11:00. The modeled $P(O_3)_{net}$ in this study was comparable
 517 to the net O_3 production rate in Wangdu in summer (Tan et al., 2017), while the net ozone production rate in Shenzhen was
 518 much higher than the gross O_3 production rate in Beijing in winter (Tan et al., 2018).

$$519 F(O_3) = k_{HO_2+NO}[HO_2][NO] + \sum_i k_{RO_2i+NO}[RO_2]_i[NO] \quad (5)$$

$$520 L(O_3) = \theta j(O^1D)[O_3] + k_{O_3+OH}[O_3][OH] + k_{O_3+HO_2}[O_3][HO_2] + (\sum(k_{alkenes+O_3}^i [alkenes^i]))[O_3] \quad (6)$$

521
$$P(O_3)_{\text{net}} = F(O_3) - L(O_3) - k_{\text{NO}_2+\text{OH}}[\text{NO}_2][\text{OH}] \quad (7)$$

522 where θ is the fraction of O^1D from ozone photolysis that reacts with water vapor.

523 Herein, we presented the NO dependence on $P(O_3)_{\text{net}}$, AOC_{VOCs} , and the ratio of $P(O_3)_{\text{net}}$ to AOC_{VOCs} in Fig. 8 (b-d), in which
524 AOC_{VOCs} denotes the atmospheric oxidation capacity only from the VOCs oxidation, which includes the channels of primary
525 VOCs (excluding OVOCs, and mainly alkanes, alkenes, aromatics and isoprene) with OH radicals. An upward trend of $P(O_3)_{\text{net}}$
526 was presented with the increase of NO concentration when NO concentration was below 1 ppb, while $P(O_3)_{\text{net}}$ decreased with
527 the increase of NO concentration because NO_2 became the sink of OH radicals gradually when NO concentration was above
528 1 ppb. In terms of the NO dependence on AOC_{VOCs} , no significant variation was found, indicating VOCs oxidation was weakly
529 impacted by NO concentrations in this campaign. Since AOC_{VOCs} can represent the VOCs oxidant rate, and thus the ratio of
530 $P(O_3)_{\text{net}}$ to AOC_{VOCs} can reflect the yield of net ozone production from VOCs oxidation. Similar to $P(O_3)_{\text{net}}$, the ratios increased
531 with the increase of NO concentration when NO concentration was below 1 ppb, while the ratios decreased with the increase
532 of NO concentration when NO concentration was above 1 ppb, indicating the yield of net O_3 production from VOCs oxidation
533 would be lower within the low NO regime (< 1 ppb) and high NO regime (> 1 ppb). The median ratios ranged from 1.0 to 4.5,
534 and the maximum of the median ratios existed when NO concentration was approximately 1 ppb, with a value of approximately
535 4.5. The nonlinear response of the yield of net ozone production to NO indicated that it is necessary to optimize the NO_x and
536 VOC control strategies for the reduction of O_3 pollution effectively.

537

538 **5 Conclusions**

539 The STORM field campaign was carried out at Shenzhen site in the autumn of 2018, providing the continuous OH and HO_2^*
540 observations in PRD since the Heshan campaign in 2014. The maximum diurnal OH and HO_2^* concentrations, which were
541 measured by PKU-LIF system, were $4.5 \times 10^6 \text{ cm}^{-3}$ and $4.2 \times 10^8 \text{ cm}^{-3}$, respectively. The observed OH concentration was equal
542 to that measured at Heshan site (autumn campaign) but was lower than those measured in summer campaigns in China
543 (Backgarden, Yufa, Wangdu, Taizhou and Chengdu sites). The observed HO_2^* concentrations included the true HO_2
544 concentrations and an estimated interference from RO_2 radicals, and was much lower than those measured at the Backgarden
545 and Yufa sites in China.

546 The base model (RACM2-LIM1) could reproduce the observed OH concentration before 10:00, and thereafter, OH was
547 underestimated by the model when NO concentration dropped to low levels. The results of the radical experimental budget
548 indicated that OH underestimation was likely attributable to an unknown missing OH source at low NO regime. We diagnosed
549 the missing OH source by sensitivity runs, and unclassical OH recycling was identified again in this study. Good agreement
550 between the modeled and observed OH concentrations was achieved when a constant mixing ratio of the numerical species X,

551 equivalent to 0.1 ppb NO, was added into the base model. Additionally, we found isoprene and OVOCs might closely influence
552 the missing OH sources by comparing the composition of VOCs reactivity under the different NO intervals. Isoprene
553 isomerization mechanism (LIM1) can explain approximately 7% of the missing OH production rate, and no significant
554 contribution of MACR and MVK oxidation was found. As another potential OH source, OVOCs species should be further
555 explored to explain the remaining missing OH sources. As for HO₂ radicals, the overestimation of HO₂^{*} concentration was
556 found, indicating that HO₂ heterogeneous uptake with the effective uptake coefficient of 0.3 might make a significant role in
557 HO₂ sinks. Good agreements of OH observations-simulations and HO₂^{*} observations-simulations were both achieved when
558 the amount of X changed from 0.1 ppb to 0.25 ppb and the HO₂ effective uptake coefficient was 0.3.

559 The quantification of production and destruction channels of ROx radicals is essential to explore the chemical processes of
560 radicals. The ROx primary production and termination rates were balanced for the entire day, with maxima of 4 ppb h⁻¹, similar
561 to those at the Heshan and Wangdu sites. Photolysis channels dominated the ROx primary production rate, and the HONO, O₃,
562 HCHO, and carbonyls photolysis accounted for 29%, 16%, 16%, and 11% during the daytime, respectively. The most fraction
563 of ROx termination rate came from the reaction of OH + NO₂ in the morning. The radical self-combination gradually became
564 the major sink of ROx in the afternoon with the decreasing of NO concentrations. The reaction of OH + NO₂ and radical self-
565 combination accounted for 35% and 24% during the daytime, respectively.

566 In this campaign, AOC exhibited well-defined diurnal patterns, with a peak of 11.8 ppb h⁻¹. As expected, OH radicals, which
567 were the dominant oxidant, accounted for 95.7% of the total AOC during the daytime. O₃ and NO₃ contributed 2.9% and 1.4%
568 to total AOC during the daytime, respectively. The ratio of $P(O_3)_{\text{net}}$ to AOC_{VOCs} , which denotes the yield of net ozone production
569 from VOCs oxidation, tended to increase and then decrease as NO concentration increased, with a range of 1.0-4.5. Optimizing
570 the NOx and VOCs control strategies might be significant to realize the reduction of ozone concentrations based on the
571 nonlinear relationship between the yield of net ozone production from VOCs oxidation and NO concentrations.

572
573 **Data availability.** The data used in this study are available from the corresponding author upon request (k.lu@pku.edu.cn).

574
575 **Author contributions.** YH Zhang and KD Lu conceived the study. XP Yang analyzed the data and wrote the manuscript with
576 inputs from KD Lu. XP Yang, XF Ma, Y Gao contributed to the measurements of the HOx concentrations. All authors
577 contributed to the discussed results and commented on the manuscript.

578
579 **Competing interests.** The authors declare that they have no conflict of interest.

580
581 **Acknowledgment.** The authors thank the science teams of the STORM-2018 campaign. This work was supported by the

582 Beijing Municipal Natural Science Foundation for Distinguished Young Scholars (JQ19031), the National Research Program
583 for Key Issue in Air Pollution Control (2019YFC0214800), and the National Natural Science Foundation of China (Grants
584 No. 91544225, 21522701, 91844301).

585 **Appendix A. Supplementary data**

586 **References**

- 587 Berndt, T., Chen, J., Kjaergaard, E. R., Moller, K. H., Tilgner, A., Hoffmann, E. H., Herrmann, H., Crounse, J. D., Wennberg,
588 P. O., and Kjaergaard, H. G.: Hydrotrioxide (ROOOH) formation in the atmosphere, *Science*, 376, 979-+,
589 10.1126/science.abn6012, 2022.
- 590 Brocco, D., Fratarcangeli, R., Lepore, L., Petricca, M., and Ventrone, I.: Determination of aromatic hydrocarbons in urban air
591 of Rome, *Atmospheric Environment*, 31, 557-566, 10.1016/s1352-2310(96)00226-9, 1997.
- 592 Chen, X., Wang, H., Liu, Y., Su, R., Wang, H., Lou, S., and Lu, K.: Spatial characteristics of the nighttime oxidation capacity
593 in the Yangtze River Delta, China, *Atmospheric Environment*, 208, 150-157, 10.1016/j.atmosenv.2019.04.012, 2019.
- 594 Ehhalt, D. H.: Photooxidation of trace gases in the troposphere, *Physical Chemistry Chemical Physics*, 1, 5401-5408,
595 10.1039/a905097c, 1999.
- 596 Elshorbany, Y. F., Kurtenbach, R., Wiesen, P., Lissi, E., Rubio, M., Villena, G., Gramsch, E., Rickard, A. R., Pilling, M. J., and
597 Kleffmann, J.: Oxidation capacity of the city air of Santiago, Chile, *Atmospheric Chemistry and Physics*, 9, 2257-2273,
598 10.5194/acp-9-2257-2009, 2009.
- 599 Fan, S., Wang, A., Fan, Q., Liu, J., and Wang, B.: ATMOSPHERIC BOUNDARY LAYER CONCEPT MODEL OF THE
600 PEARL RIVER DELTA AND ITS APPLICATION, *Journal of Tropical Meteorology*, 21, 286-292, 2005.
- 601 Feng, T., Zhao, S. Y., Hu, B., Bei, N. F., Zhang, X., Wu, J. R., Li, X., Liu, L., Wang, R. N., Tie, X. X., and Li, G. H.: Assessment
602 of Atmospheric Oxidizing Capacity Over the Beijing-Tianjin-Hebei (BTH) Area, China, *Journal of Geophysical Research-*
603 *Atmospheres*, 126, 18, 10.1029/2020jd033834, 2021.
- 604 Fittschen, C.: The reaction of peroxy radicals with OH radicals, *Chemical Physics Letters*, 725, 102-108,
605 10.1016/j.cplett.2019.04.002, 2019.
- 606 Fittschen, C., Al Ajami, M., Batut, S., Ferracci, V., Archer-Nicholls, S., Archibald, A. T., and Schoemaeker, C.: ROOOH: a
607 missing piece of the puzzle for OH measurements in low-NO environments?, *Atmospheric Chemistry and Physics*, 19, 349-
608 362, 10.5194/acp-19-349-2019, 2019.
- 609 Fuchs, H., Holland, F., and Hofzumahaus, A.: Measurement of tropospheric RO₂ and HO₂ radicals by a laser-induced
610 fluorescence instrument, *Review of Scientific Instruments*, 79, 10.1063/1.2968712, 2008.
- 611 Fuchs, H., Bohn, B., Hofzumahaus, A., Holland, F., Lu, K. D., Nehr, S., Rohrer, F., and Wahner, A.: Detection of HO₂ by laser-
612 induced fluorescence: calibration and interferences from RO₂ radicals, *Atmospheric Measurement Techniques*, 4, 1209-1225,
613 10.5194/amt-4-1209-2011, 2011.
- 614 Fuchs, H., Acir, I. H., Bohn, B., Brauers, T., Dorn, H. P., Häseler, R., Hofzumahaus, A., Holland, F., Kaminski, M., Li, X., Lu,
615 K., Lutz, A., Nehr, S., Rohrer, F., Tillmann, R., Wegener, R., and Wahner, A.: OH regeneration from methacrolein oxidation
616 investigated in the atmosphere simulation chamber SAPHIR, *Atmos. Chem. Phys.*, 14, 7895-7908, 10.5194/acp-14-7895-2014,
617 2014.
- 618 Fuchs, H., Tan, Z., Hofzumahaus, A., Broch, S., Dorn, H.-P., Holland, F., Kuenstler, C., Gomm, S., Rohrer, F., Schrade, S.,
619 Tillmann, R., and Wahner, A.: Investigation of potential interferences in the detection of atmospheric RO_x radicals by laser-
620 induced fluorescence under dark conditions, *Atmospheric Measurement Techniques*, 9, 1431-1447, 10.5194/amt-9-1431-2016,
621 2016.
- 622 Fuchs, H., Tan, Z., Lu, K., Bohn, B., Broch, S., Brown, S. S., Dong, H., Gomm, S., Haeseler, R., He, L., Hofzumahaus, A.,
623 Holland, F., Li, X., Liu, Y., Lu, S., Min, K.-E., Rohrer, F., Shao, M., Wang, B., Wang, M., Wu, Y., Zeng, L., Zhang, Y., Wahner,

624 A., and Zhang, Y.: OH reactivity at a rural site (Wangdu) in the North China Plain: contributions from OH reactants and
625 experimental OH budget, *Atmospheric Chemistry and Physics*, 17, 645-661, 10.5194/acp-17-645-2017, 2017.

626 Fuchs, H., Albrecht, S., Acir, I.-H., Bohn, B., Breitenlechner, M., Dorn, H.-P., Gkatzelis, G. I., Hofzumahaus, A., Holland, F.,
627 Kaminski, M., Keutsch, F. N., Novelli, A., Reimer, D., Rohrer, F., Tillmann, R., Vereecken, L., Wegener, R., Zaytsev, A.,
628 Kiendler-Scharr, A., and Wahner, A.: Investigation of the oxidation of methyl vinyl ketone (MVK) by OH radicals in the
629 atmospheric simulation chamber SAPHIR, *Atmospheric Chemistry and Physics*, 18, 8001-8016, 10.5194/acp-18-8001-2018,
630 2018.

631 Gao, M., Li, H., Li, Y., Wei, J., Sun, Y., He, L., and Huang, X.: Source characteristics of water-soluble organic matters in
632 PM_{2.5} in the winter of Shenzhen, *China Environmental Science*, 38, 4017-4022, 2018.

633 Geyer, A., Alicke, B., Konrad, S., Schmitz, T., Stutz, J., and Platt, U.: Chemistry and oxidation capacity of the nitrate radical
634 in the continental boundary layer near Berlin, *Journal of Geophysical Research-Atmospheres*, 106, 8013-8025,
635 10.1029/2000jd900681, 2001.

636 Heard, D. E., and Pilling, M. J.: Measurement of OH and HO₂ in the troposphere, *Chemical Reviews*, 103, 5163-5198,
637 10.1021/cr020522s, 2003.

638 Hofzumahaus, A., Aschmutat, U., Hessling, M., Holland, F., and Ehhalt, D. H.: The measurement of tropospheric OH radicals
639 by laser-induced fluorescence spectroscopy during the POPCORN field campaign, *Geophysical Research Letters*, 23, 2541-
640 2544, 10.1029/96gl02205, 1996.

641 Hofzumahaus, A., Rohrer, F., Lu, K., Bohn, B., Brauers, T., Chang, C.-C., Fuchs, H., Holland, F., Kita, K., Kondo, Y., Li, X.,
642 Lou, S., Shao, M., Zeng, L., Wahner, A., and Zhang, Y.: Amplified Trace Gas Removal in the Troposphere, *Science*, 324, 1702-
643 1704, 10.1126/science.1164566, 2009.

644 Holland, F., Hessling, M., and Hofzumahaus, A.: IN-SITU MEASUREMENT OF TROPOSPHERIC OH RADICALS BY
645 LASER-INDUCED FLUORESCENCE - A DESCRIPTION OF THE KFA INSTRUMENT, *Journal of the Atmospheric
646 Sciences*, 52, 3393-3401, 10.1175/1520-0469(1995)052<3393:ismoto>2.0.Co;2, 1995.

647 Huang, X.-F., Chen, D.-L., Lan, Z.-J., Feng, N., He, L.-Y., Yu, G.-H., and Luan, S.-J.: Characterization of organic aerosol in
648 fine particles in a mega-city of South China: Molecular composition, seasonal variation, and size distribution, *Atmospheric
649 Research*, 114-115, 28-37, <https://doi.org/10.1016/j.atmosres.2012.05.019>, 2012a.

650 Huang, X.-F., Sun, T.-L., Zeng, L.-W., Yu, G.-H., and Luan, S.-J.: Black carbon aerosol characterization in a coastal city in
651 South China using a single particle soot photometer, *Atmospheric Environment*, 51, 21-28,
652 <https://doi.org/10.1016/j.atmosenv.2012.01.056>, 2012b.

653 Jones, C. E., Hopkins, J. R., and Lewis, A. C.: In situ measurements of isoprene and monoterpenes within a south-east Asian
654 tropical rainforest, *Atmospheric Chemistry and Physics*, 11, 6971-6984, 10.5194/acp-11-6971-2011, 2011.

655 Kanaya, Y., Sadanaga, Y., Matsumoto, J., Sharma, U. K., Hirokawa, J., Kajii, Y., and Akimoto, H.: Daytime HO₂ concentrations
656 at Oki Island, Japan, in summer 1998: Comparison between measurement and theory, *Journal of Geophysical Research-
657 Atmospheres*, 105, 24205-24222, 10.1029/2000jd900308, 2000.

658 Kanaya, Y., Cao, R., Kato, S., Miyakawa, Y., Kajii, Y., Tanimoto, H., Yokouchi, Y., Mochida, M., Kawamura, K., and Akimoto,
659 H.: Chemistry of OH and HO₂ radicals observed at Rishiri Island, Japan, in September 2003: Missing daytime sink of HO₂
660 and positive nighttime correlations with monoterpenes, *Journal of Geophysical Research-Atmospheres*, 112,
661 10.1029/2006jd007987, 2007.

662 Lelieveld, J., Butler, T. M., Crowley, J. N., Dillon, T. J., Fischer, H., Ganzeveld, L., Harder, H., Lawrence, M. G., Martinez,
663 M., Taraborrelli, D., and Williams, J.: Atmospheric oxidation capacity sustained by a tropical forest, *Nature*, 452, 737-740,
664 10.1038/nature06870, 2008.

665 Levy, H.: NORMAL ATMOSPHERE - LARGE RADICAL AND FORMALDEHYDE CONCENTRATIONS PREDICTED,
666 *Science*, 173, 141-&, 10.1126/science.173.3992.141, 1971.

667 Li, K., Jacob, D. J., Liao, H., Shen, L., Zhang, Q., and Bates, K. H.: Anthropogenic drivers of 2013-2017 trends in summer
668 surface ozone in China, *Proceedings of the National Academy of Sciences of the United States of America*, 116, 422-427,
669 10.1073/pnas.1812168116, 2019.

670 Li, Z., Xue, L., Yang, X., Zha, Q., Tham, Y. J., Yan, C., Louie, P. K. K., Luk, C. W. Y., Wang, T., and Wang, W.: Oxidizing

671 capacity of the rural atmosphere in Hong Kong, Southern China, *Science of the Total Environment*, 612, 1114-1122,
672 10.1016/j.scitotenv.2017.08.310, 2018.

673 Liu, S., Li, X., Shen, X., Zeng, L., Huang, X., Zhu, B., Lin, L., and Lou, S.: Measurement and partition analysis of atmospheric
674 OH reactivity in autumn in Shenzhen, *Acta Scientiae Circumstantiae*, 39, 3600-3610, 2019.

675 Liu, Z., Wang, Y., Hu, B., Lu, K., Tang, G., Ji, D., Yang, X., Gao, W., Xie, Y., Liu, J., Yao, D., Yang, Y., and Zhang, Y.:
676 Elucidating the quantitative characterization of atmospheric oxidation capacity in Beijing, China, *Science of the Total
677 Environment*, 771, 10.1016/j.scitotenv.2021.145306, 2021.

678 Lou, S., Holland, F., Rohrer, F., Lu, K., Bohn, B., Brauers, T., Chang, C. C., Fuchs, H., Haeseler, R., Kita, K., Kondo, Y., Li,
679 X., Shao, M., Zeng, L., Wahner, A., Zhang, Y., Wang, W., and Hofzumahaus, A.: Atmospheric OH reactivities in the Pearl
680 River Delta - China in summer 2006: measurement and model results, *Atmospheric Chemistry and Physics*, 10, 11243-11260,
681 10.5194/acp-10-11243-2010, 2010.

682 Lu, K., Guo, S., Tan, Z., Wang, H., Shang, D., Liu, Y., Li, X., Wu, Z., Hu, M., and Zhang, Y.: Exploring atmospheric free-
683 radical chemistry in China: the self-cleansing capacity and the formation of secondary air pollution, *National Science Review*,
684 6, 579-594, 10.1093/nsr/nwy073, 2019.

685 Lu, K. D., Rohrer, F., Holland, F., Fuchs, H., Bohn, B., Brauers, T., Chang, C. C., Haeseler, R., Hu, M., Kita, K., Kondo, Y.,
686 Li, X., Lou, S. R., Nehr, S., Shao, M., Zeng, L. M., Wahner, A., Zhang, Y. H., and Hofzumahaus, A.: Observation and modelling
687 of OH and HO₂ concentrations in the Pearl River Delta 2006: a missing OH source in a VOC rich atmosphere, *Atmospheric
688 Chemistry and Physics*, 12, 1541-1569, 10.5194/acp-12-1541-2012, 2012.

689 Lu, K. D., Hofzumahaus, A., Holland, F., Bohn, B., Brauers, T., Fuchs, H., Hu, M., Haeseler, R., Kita, K., Kondo, Y., Li, X.,
690 Lou, S. R., Oebel, A., Shao, M., Zeng, L. M., Wahner, A., Zhu, T., Zhang, Y. H., and Rohrer, F.: Missing OH source in a
691 suburban environment near Beijing: observed and modelled OH and HO₂ concentrations in summer 2006, *Atmospheric
692 Chemistry and Physics*, 13, 1057-1080, 10.5194/acp-13-1057-2013, 2013.

693 Ma, X., Tan, Z., Lu, K., Yang, X., Liu, Y., Li, S., Li, X., Chen, S., Novelli, A., Cho, C., Zeng, L., Wahner, A., and Zhang, Y.:
694 Winter photochemistry in Beijing: Observation and model simulation of OH and HO₂ radicals at an urban site, *Science of the
695 Total Environment*, 685, 85-95, 10.1016/j.scitotenv.2019.05.329, 2019a.

696 Ma, X., Tan, Z., Lu, K., Yang, X., Chen, X., Wang, H., Chen, S., Fang, X., Li, S., Li, X., Liu, J., Liu, Y., Lou, S., Qiu, W.,
697 Wang, H., Zeng, L., and Zhang, Y.: OH and HO₂ radical chemistry at a suburban site during the EXPLORE-YRD campaign
698 in 2018, *Atmospheric Chemistry and Physics*, 22, 7005-7028, 10.5194/acp-22-7005-2022, 2022a.

699 Ma, X. F., Tan, Z. F., Lu, K. D., Yang, X. P., Chen, X. R., Wang, H. C., Chen, S. Y., Fang, X., Li, S. L., Li, X., Liu, J. W., Liu,
700 Y., Lou, S. R., Qiu, W. Y., Wang, H. L., Zeng, L. M., and Zhang, Y. H.: OH and HO₂ radical chemistry at a suburban site during
701 the EXPLORE-YRD campaign in 2018, *Atmospheric Chemistry and Physics*, 22, 7005-7028, 10.5194/acp-22-7005-2022,
702 2022b.

703 Ma, X. Y., Jia, H. L., Sha, T., An, J. L., and Tian, R.: Spatial and seasonal characteristics of particulate matter and gaseous
704 pollution in China: Implications for control policy, *Environmental Pollution*, 248, 421-428, 10.1016/j.envpol.2019.02.038,
705 2019b.

706 Mao, J., Jacob, D. J., Evans, M. J., Olson, J. R., Ren, X., Brune, W. H., St Clair, J. M., Crounse, J. D., Spencer, K. M., Beaver,
707 M. R., Wennberg, P. O., Cubison, M. J., Jimenez, J. L., Fried, A., Weibring, P., Walega, J. G., Hall, S. R., Weinheimer, A. J.,
708 Cohen, R. C., Chen, G., Crawford, J. H., McNaughton, C., Clarke, A. D., Jaegle, L., Fisher, J. A., Yantosca, R. M., Le Sager,
709 P., and Carouge, C.: Chemistry of hydrogen oxide radicals (HO_x) in the Arctic troposphere in spring, *Atmospheric Chemistry
710 and Physics*, 10, 5823-5838, 10.5194/acp-10-5823-2010, 2010.

711 Mao, J., Ren, X., Zhang, L., Van Duin, D. M., Cohen, R. C., Park, J. H., Goldstein, A. H., Paulot, F., Beaver, M. R., Crounse,
712 J. D., Wennberg, P. O., DiGangi, J. P., Henry, S. B., Keutsch, F. N., Park, C., Schade, G. W., Wolfe, G. M., Thornton, J. A., and
713 Brune, W. H.: Insights into hydroxyl measurements and atmospheric oxidation in a California forest, *Atmospheric Chemistry
714 and Physics*, 12, 8009-8020, 10.5194/acp-12-8009-2012, 2012.

715 Novelli, A., Hens, K., Ernest, C. T., Kubistin, D., Regelin, E., Elste, T., Plass-Duelmer, C., Martinez, M., Lelieveld, J., and
716 Harder, H.: Characterisation of an inlet pre-injector laser-induced fluorescence instrument for the measurement of atmospheric
717 hydroxyl radicals, *Atmospheric Measurement Techniques*, 7, 3413-3430, 10.5194/amt-7-3413-2014, 2014.

718 Peeters, J., Nguyen, T. L., and Vereecken, L.: HOx radical regeneration in the oxidation of isoprene, *Physical Chemistry*
719 *Chemical Physics*, 11, 5935-5939, 10.1039/b908511d, 2009.

720 Peeters, J., and Muller, J.-F.: HOx radical regeneration in isoprene oxidation via peroxy radical isomerisations. II: experimental
721 evidence and global impact, *Physical Chemistry Chemical Physics*, 12, 14227-14235, 10.1039/c0cp00811g, 2010.

722 Peeters, J., Muller, J.-F., Stavrou, T., and Vinh Son, N.: Hydroxyl Radical Recycling in Isoprene Oxidation Driven by
723 Hydrogen Bonding and Hydrogen Tunneling: The Upgraded LIM1 Mechanism, *Journal of Physical Chemistry A*, 118, 8625-
724 8643, 10.1021/jp5033146, 2014.

725 Ren, X., Olson, J. R., Crawford, J. H., Brune, W. H., Mao, J., Long, R. B., Chen, Z., Chen, G., Avery, M. A., Sachse, G. W.,
726 Barrick, J. D., Diskin, G. S., Huey, L. G., Fried, A., Cohen, R. C., Heikes, B., Wennberg, P. O., Singh, H. B., Blake, D. R., and
727 Shetter, R. E.: HOx chemistry during INTEX-A 2004: Observation, model calculation, and comparison with previous studies,
728 *Journal of Geophysical Research-Atmospheres*, 113, 10.1029/2007jd009166, 2008.

729 Shu, L., Wang, T. J., Han, H., Xie, M., Chen, P. L., Li, M. M., and Wu, H.: Summertime ozone pollution in the Yangtze River
730 Delta of eastern China during 2013-2017: Synoptic impacts and source apportionment, *Environmental Pollution*, 257,
731 10.1016/j.envpol.2019.113631, 2020.

732 Song, H., Zou, Q., and Lu, K.: Parameterization and Application of Hydroperoxyl Radicals (HO₂) Heterogeneous Uptake
733 Coefficient, *Progress in Chemistry*, 33, 1161-1173, 10.7536/pc200749, 2021.

734 Song, H., Lu, K., Dong, H., Tan, Z., Chen, S., Zeng, L., and Zhang, Y.: Reduced Aerosol Uptake of Hydroperoxyl Radical May
735 Increase the Sensitivity of Ozone Production to Volatile Organic Compounds, *Environmental Science & Technology Letters*,
736 9, 22-29, 10.1021/acs.estlett.1c00893, 2022.

737 Stevens, P. S., Mather, J. H., Brune, W. H., Eisele, F., Tanner, D., Jefferson, A., Cantrell, C., Shetter, R., Sewall, S., Fried, A.,
738 Henry, B., Williams, E., Baumann, K., Goldan, P., and Kuster, W.: HO₂/OH and RO(2)/HO₂ ratios during the Tropospheric
739 OH Photochemistry Experiment: Measurement and theory, *Journal of Geophysical Research-Atmospheres*, 102, 6379-6391,
740 10.1029/96jd01704, 1997.

741 Stone, D., Whalley, L. K., and Heard, D. E.: Tropospheric OH and HO₂ radicals: field measurements and model comparisons,
742 *Chemical Society Reviews*, 41, 6348-6404, 10.1039/c2cs35140d, 2012.

743 Stone, D., Evans, M. J., Walker, H., Ingham, T., Vaughan, S., Ouyang, B., Kennedy, O. J., McLeod, M. W., Jones, R. L.,
744 Hopkins, J., Punjabi, S., Lidster, R., Hamilton, J. F., Lee, J. D., Lewis, A. C., Carpenter, L. J., Forster, G., Oram, D. E., Reeves,
745 C. E., Bauguitte, S., Morgan, W., Coe, H., Aruffo, E., Dari-Salisburgo, C., Giammaria, F., Di Carlo, P., and Heard, D. E.:
746 Radical chemistry at night: comparisons between observed and modelled HOx, NO₃ and N₂O₅ during the RONOCO project,
747 *Atmospheric Chemistry and Physics*, 14, 1299-1321, 10.5194/acp-14-1299-2014, 2014.

748 Taketani, F., Kanaya, Y., Pochanart, P., Liu, Y., Li, J., Okuzawa, K., Kawamura, K., Wang, Z., and Akimoto, H.: Measurement
749 of overall uptake coefficients for HO₂ radicals by aerosol particles sampled from ambient air at Mts. Tai and Mang (China),
750 *Atmospheric Chemistry and Physics*, 12, 11907-11916, 10.5194/acp-12-11907-2012, 2012.

751 Tan, Z., Fuchs, H., Lu, K., Hofzumahaus, A., Bohn, B., Broch, S., Dong, H., Gomm, S., Haeseler, R., He, L., Holland, F., Li,
752 X., Liu, Y., Lu, S., Rohrer, F., Shao, M., Wang, B., Wang, M., Wu, Y., Zeng, L., Zhang, Y., Wahner, A., and Zhang, Y.: Radical
753 chemistry at a rural site (Wangdu) in the North China Plain: observation and model calculations of OH, HO₂ and RO₂ radicals,
754 *Atmospheric Chemistry and Physics*, 17, 663-690, 10.5194/acp-17-663-2017, 2017.

755 Tan, Z., Rohrer, F., Lu, K., Ma, X., Bohn, B., Broch, S., Dong, H., Fuchs, H., Gkatzelis, G. I., Hofzumahaus, A., Holland, F.,
756 Li, X., Liu, Y., Liu, Y., Novelli, A., Shao, M., Wang, H., Wu, Y., Zeng, L., Hu, M., Kiendler-Scharr, A., Wahner, A., and Zhang,
757 Y.: Wintertime photochemistry in Beijing: observations of ROx radical concentrations in the North China Plain during the
758 BEST-ONE campaign, *Atmospheric Chemistry and Physics*, 18, 12391-12411, 10.5194/acp-18-12391-2018, 2018.

759 Tan, Z., Lu, K., Hofzumahaus, A., Fuchs, H., Bohn, B., Holland, F., Liu, Y., Rohrer, F., Shao, M., Sun, K., Wu, Y., Zeng, L.,
760 Zhang, Y., Zou, Q., Kiendler-Scharr, A., Wahner, A., and Zhang, Y.: Experimental budgets of OH, HO₂, and RO₂ radicals and
761 implications for ozone formation in the Pearl River Delta in China 2014, *Atmospheric Chemistry and Physics*, 19, 7129-7150,
762 10.5194/acp-19-7129-2019, 2019.

763 Tan, Z., Hofzumahaus, A., Lu, K., Brown, S. S., Holland, F., Huey, L. G., Kiendler-Scharr, A., Li, X., Liu, X., Ma, N., Min,
764 K.-E., Rohrer, F., Shao, M., Wahner, A., Wang, Y., Wiedensohler, A., Wu, Y., Wu, Z., Zeng, L., Zhang, Y., and Fuchs, H.: No

765 Evidence for a Significant Impact of Heterogeneous Chemistry on Radical Concentrations in the North China Plain in Summer
766 2014, *Environmental Science & Technology*, 54, 5973-5979, 10.1021/acs.est.0c00525, 2020.

767 Tan, Z., Ma, X., Lu, K., Jiang, M., Zou, Q., Wang, H., Zeng, L., and Zhang, Y.: Direct evidence of local photochemical
768 production driven ozone episode in Beijing: A case study, *Science of the Total Environment*, 800,
769 10.1016/j.scitotenv.2021.148868, 2021.

770 Wang, T., Xue, L. K., Brimblecombe, P., Lam, Y. F., Li, L., and Zhang, L.: Ozone pollution in China: A review of concentrations,
771 meteorological influences, chemical precursors, and effects, *Science of the Total Environment*, 575, 1582-1596,
772 10.1016/j.scitotenv.2016.10.081, 2017a.

773 Wang, W., Parrish, D. D., Li, X., Shao, M., Liu, Y., Mo, Z., Lu, S., Hu, M., Fang, X., Wu, Y., Zeng, L., and Zhang, Y.: Exploring
774 the drivers of the increased ozone production in Beijing in summertime during 2005-2016, *Atmospheric Chemistry and Physics*,
775 20, 15617-15633, 10.5194/acp-20-15617-2020, 2020.

776 Wang, X., Wang, H., Xue, L., Wang, T., Wang, L., Gu, R., Wang, W., Tham, Y. J., Wang, Z., Yang, L., Chen, J., and Wang, W.:
777 Observations of N₂O₅ and ClNO₂ at a polluted urban surface site in North China: High N₂O₅ uptake coefficients and low
778 ClNO₂ product yields, *Atmospheric Environment*, 156, 125-134, 10.1016/j.atmosenv.2017.02.035, 2017b.

779 Whalley, L. K., Edwards, P. M., Furneaux, K. L., Goddard, A., Ingham, T., Evans, M. J., Stone, D., Hopkins, J. R., Jones, C.
780 E., Karunaharan, A., Lee, J. D., Lewis, A. C., Monks, P. S., Moller, S. J., and Heard, D. E.: Quantifying the magnitude of a
781 missing hydroxyl radical source in a tropical rainforest, *Atmospheric Chemistry and Physics*, 11, 7223-7233, 10.5194/acp-11-
782 7223-2011, 2011.

783 Whalley, L. K., Stone, D., George, I. J., Mertes, S., van Pinxteren, D., Tilgner, A., Herrmann, H., Evans, M. J., and Heard, D.
784 E.: The influence of clouds on radical concentrations: observations and modelling studies of HO_x during the Hill Cap Cloud
785 Thuringia (HCCT) campaign in 2010, *Atmospheric Chemistry and Physics*, 15, 3289-3301, 10.5194/acp-15-3289-2015, 2015.

786 Whalley, L. K., Slater, E. J., Woodward-Massey, R., Ye, C., Lee, J. D., Squires, F., Hopkins, J. R., Dunmore, R. E., Shaw, M.,
787 Hamilton, J. F., Lewis, A. C., Mehra, A., Worrall, S. D., Bacak, A., Bannan, T. J., Coe, H., Percival, C. J., Ouyang, B., Jones,
788 R. L., Crilley, L. R., Kramer, L. J., Bloss, W. J., Vu, T., Kotthaus, S., Grimmond, S., Sun, Y., Xu, W., Yue, S., Ren, L., Acton,
789 W. J. F., Hewitt, C. N., Wang, X., Fu, P., and Heard, D. E.: Evaluating the sensitivity of radical chemistry and ozone formation
790 to ambient VOCs and NO_x in Beijing, *Atmospheric Chemistry and Physics*, 21, 2125-2147, 10.5194/acp-21-2125-2021, 2021.

791 Xue, L., Gu, R., Wang, T., Wang, X., Saunders, S., Blake, D., Louie, P. K. K., Luk, C. W. Y., Simpson, I., Xu, Z., Wang, Z.,
792 Gao, Y., Lee, S., Mellouki, A., and Wang, W.: Oxidative capacity and radical chemistry in the polluted atmosphere of Hong
793 Kong and Pearl River Delta region: analysis of a severe photochemical smog episode, *Atmospheric Chemistry and Physics*,
794 16, 9891-9903, 10.5194/acp-16-9891-2016, 2016.

795 Yang, X., Wang, H., Tan, Z., Lu, K., and Zhang, Y.: Observations of OH Radical Reactivity in Field Studies, *Acta Chimica*
796 *Sinica*, 77, 613-624, 10.6023/a19030094, 2019.

797 Yang, X., Lu, K., Ma, X., Liu, Y., Wang, H., Hu, R., Li, X., Lou, S., Chen, S., Dong, H., Wang, F., Wang, Y., Zhang, G., Li, S.,
798 Yang, S., Yang, Y., Kuang, C., Tan, Z., Chen, X., Qiu, P., Zeng, L., Xie, P., and Zhang, Y.: Observations and modeling of OH
799 and HO₂ radicals in Chengdu, China in summer 2019, *The Science of the total environment*, 772, 144829-144829,
800 10.1016/j.scitotenv.2020.144829, 2021.

801 Yang, Y., Wang, Y., Yao, D., Zhao, S., Yang, S., Ji, D., Sun, J., Wang, Y., Liu, Z., Hu, B., Zhang, R., and Wang, Y.: Significant
802 decreases in the volatile organic compound concentration, atmospheric oxidation capacity and photochemical reactivity during
803 the National Day holiday over a suburban site in the North China Plain, *Environmental Pollution*, 263,
804 10.1016/j.envpol.2020.114657, 2020a.

805 Yang, Y., Wang, Y., Yao, D., Zhao, S., Yang, S., Ji, D., Sun, J., Wang, Y., Liu, Z., Hu, B., Zhang, R., and Wang, Y.: Significant
806 decreases in the volatile organic compound concentration, atmospheric oxidation capacity and photochemical reactivity during
807 the National Day holiday over a suburban site in the North China Plain, *Environmental Pollution*, 263, 114657,
808 <https://doi.org/10.1016/j.envpol.2020.114657>, 2020b.

809 Yu, D., Tan, Z., Lu, K., Ma, X., Li, X., Chen, S., Zhu, B., Lin, L., Li, Y., Qiu, P., Yang, X., Liu, Y., Wang, H., He, L., Huang,
810 X., and Zhang, Y.: An explicit study of local ozone budget and NO_x-VOCs sensitivity in Shenzhen China, *Atmospheric*
811 *Environment*, 224, 117304, <https://doi.org/10.1016/j.atmosenv.2020.117304>, 2020.

812 Zhang, Y. H., Hu, M., Zhong, L. J., Wiedensohler, A., Liu, S. C., Andreae, M. O., Wang, W., and Fan, S. J.: Regional Integrated
813 Experiments on Air Quality over Pearl River Delta 2004 (PRIDE-PRD2004): Overview, *Atmospheric Environment*, 42, 6157-
814 6173, 10.1016/j.atmosenv.2008.03.025, 2008.

815 Zhou, J., Murano, K., Kohno, N., Sakamoto, Y., and Kajii, Y.: Real-time quantification of the total HO₂ reactivity of ambient
816 air and HO₂ uptake kinetics onto ambient aerosols in Kyoto (Japan), *Atmospheric Environment*, 223,
817 10.1016/j.atmosenv.2020.117189, 2020.

818 Zhou, J., Sato, K., Bai, Y., Fukusaki, Y., Kousa, Y., Ramasamy, S., Takami, A., Yoshino, A., Nakayama, T., Sadanaga, Y.,
819 Nakashima, Y., Li, J., Murano, K., Kohno, N., Sakamoto, Y., and Kajii, Y.: Kinetics and impacting factors of HO₂ uptake onto
820 submicron atmospheric aerosols during the 2019 Air QUALity Study (AQUAS) in Yokohama, Japan, *Atmospheric Chemistry
821 and Physics*, 21, 12243-12260, 10.5194/acp-21-12243-2021, 2021.

822 Zhu, J., Wang, S., Wang, H., Jing, S., Lou, S., Saiz-Lopez, A., and Zhou, B.: Observationally constrained modeling of
823 atmospheric oxidation capacity and photochemical reactivity in Shanghai, China, *Atmospheric Chemistry and Physics*, 20,
824 1217-1232, 10.5194/acp-20-1217-2020, 2020.

825